NTNU
**Norwegian University of
Science and Technology**

Detecting Anomalies and Water Distribution in Railway Ballast Using GPR

Pål Arne Ytrehus Ibrekk

Civil and Environmental Engineering
Submission date: December 2015
Supervisor: Elias Kassa, BAT

Norwegian University of Science and Technology
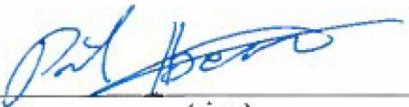Department of Civil and Transport Engineering

NORGES TEKNISK-
NATURVITENSKAPELIGE UNIVERSITET
INSTITUTT FOR BYGG, ANLEGG OG TRANSPORT

Oppgavens tittel: Detecting Anomalies and Water Distribution in Railway Ballast Using GPR	Dato: 15. Desember 2015		
	Antall sider (inkl. bilag): 103		
	Masteroppgave	X	Prosjektoppgave

Navn: Pål Arne Ytrehus Ibrekk
Faglærer/veileder: Elias Kassa
Eventuelle eksterne faglige kontakter/veiledere: Margareta Viklund, Jernbaneverket

Ekstrakt:

Ground Penetrating Radar has seen increased interest in recent years as an efficient non-destructive method of railway track surveying. As a response, it is necessary to establish the scope of its abilities for this application.

The purpose of this thesis is to assess the abilities of a GPR system to detect anomalies like ballast pockets, and to map the distribution of water in railway ballast. In addition, the thesis itself is meant to serve as a comprehensible introduction to the field of GPR surveying, as well as an update on the latest research on its railway applications.

The work has consisted of an extensive literature review and field tests performed on a live railway track.

Literary sources describe GPR as a versatile system, with many areas of application and significant advantages over current inspection methods. Ballast thickness, fouling levels and buried objects can all be detected with relative ease, and recent advantages in data processing techniques have expanded the scope of applications further.

Field surveys confirmed the utilised GPR-system's abilities to accurately detect several subsurface track anomalies, and all the necessary features to reveal ballast pocket occurrence. This was accomplished with a minimal level of system customisation and post-processing of data.

Water distribution mapping abilities were indicated from the literature review, however, field study results were only partly conclusive due to unfavourable testing conditions (rain). While the test results seemed to indicate the waters propagation, the GPR's abilities could not be decisively confirmed.

Further studies are recommended to confirm the findings of this thesis and to further explore the scope of railway applications for GPR systems.

Stikkord:

1. Ground Penetrating Radar
2. Ballast pocket
3. Water distribution
4. Ballast inspection

(sign.)

NTNU
**Norwegian University of
Science and Technology**

Detecting Anomalies and Water Distribution in Railway Ballast Using GPR

Pål Arne Ytrehus Ibrekk

December 2015

MASTER'S THESIS

TBA 4955

Department of Civil and Transport Engineering

Norwegian University of Science and Technology

Supervisor: Professor Elias Kassa
Co-supervisor: Margareta Viklund

Preface

This is a Master's thesis on railway applications of Ground Penetrating Radar, performed as part of the Railway Engineering program at NTNU during the fall semester of 2015. The work has been both engaging and educational. Starting from never having heard about Ground Penetrating Radar in August, to completion of this study in December.

The scope of the study is based on the specifications of Work Package 1 of the EU's DESTination RAIL research project. It is the hope of the author that this thesis will work to advance the field of GPR track surveying, and that it may serve as a comprehensible source of information regarding the opportunities and limitations of this technology.

The reader is assumed to possess a basic understanding of railway engineering and physics. Relevant technical acronyms are listed at the beginning of the thesis.

Technical equipment, guidance and personnel for surveying and analysis have been provided by NTNU.
Jernbaneverket has also contributed with equipment, personnel and track access for the practical field test.

The author wishes to thank:
Professor Elias Kassa for supervising my work, helping to shape the scope of the thesis.
Dr. Anne Lalagüe for help and insight in the collection and analysis of the GPR data.
Dr. Emilie Guegan for help in the laboratory and on the field test.
Jan Erik Molde and *Bent Lervik* for technical assistance with the GPR equipment.
Margareta Viklund for assistance in organising the field test.

Trondheim, Fall 2015
Pål Arne Ytrehus Ibrekk

Abstract

Ground Penetrating Radar has seen increased interest in recent years as an efficient non-destructive method of railway track surveying. As a response, it is necessary to establish the scope of its abilities for this application.

The purpose of this thesis is to assess the abilities of a GPR system to detect anomalies like ballast pockets, and to map the distribution of water in railway ballast. In addition, the thesis itself is meant to serve as a comprehensible introduction to the field of GPR surveying, as well as an update on the latest research on its railway applications.

The work has consisted of an extensive literature review and field tests performed on a live railway track.

Literary sources describe GPR as a versatile system, with many areas of application and significant advantages over current inspection methods. Ballast thickness, fouling levels and buried objects can all be detected with relative ease, and recent advantages in data processing techniques have expanded the scope of applications further.

Field surveys confirmed the utilised GPR-system's abilities to accurately detect several subsurface track anomalies, and all the necessary features to reveal ballast pocket occurrence. This was accomplished with a minimal level of system customisation and post-processing of data.

Water distribution mapping abilities were indicated from the literature review, however, field study results were only partly conclusive due to unfavourable testing conditions (rain). While the test results seemed to indicate the waters propagation, the GPR's abilities could not be decisively confirmed.

Further studies are recommended to confirm the findings of this thesis and to further explore the scope of railway applications for GPR systems.

Sammendrag

Georadar har fått stadig økende oppmerksomhet som en effektiv ikke-destruktiv metode for tilstandvurdering av jernbanespor. Som følge av dette er det nødvendig å avklare mulighetene og begrensningene ved dette systemet og bruksområdet.

Formålet med denne studien er å vurdere georadar-systemets evne til å oppdage feil i sporkroppen som ballastlommer, og til å kartlegge fordelingen av vann i ballasten. I tillegg er studien i seg selv ment å kunne brukes som en faglig introduksjon til georadarundersøkelser av jernbanespor, samt en oppdatering på den seneste forskningen på området.

Arbeidet har bestått av et omfattende litteraturstudie og feltforsøk utført på et aktivt jernbanespor.

Litterære kilder beskriver georadar som et allsidig system, med mange anvendelsesområder og betydelige fortrinn over tradisjonelle inspeksjonsmetoder. Ballasttykkelse, -forurensning og skjulte gjenstander kan oppdages relativt enkelt, og nylige fremskritt innen databehandling har videre utvidet bruksområdene.

Feltforsøkene bekreftet georadarens evne til å presist identifisere flere uregelmessigheter i sporkroppen, og alle egenskapene nødvendig for å oppdage ballastlommer ble bekreftet. Dette ble oppnådd med minimal grad av tilpasning av systemet og etterbehandling av data.

Georadarens evne til å kartlegge vannfordelingen i ballasten ble antydet i litteraturen, men resultatene av feltforsøkene var ikke helt entydige på grunn av uheldige forhold rundt testen (regn). Selv om resultatene virket å antyde vannets bevegelse kunne ikke georadarens evner på dette området fullstendig bekreftes.

Det anbefales at videre studier gjøres for å bekreftene funnene som er gjort i denne studien. Muligheter og begrensninger ved georadarundersøkelser av jernbanespor burde kartlegges videre.

Acronyms

GPR   Ground Penetrating Radar

EM   Electromagnetic

CMP   Common Midpoint test

CRS   Common Reflection Surface test

STFT   Short-Time Fourier Transform

ZOP   Zone of Penetration

DMI   Distance Measuring Instrument

NDT   Non-Destructive Testing

Contents

List of Figures

List of Tables

1 Introduction

Operation and maintenance of ballasted railway tracks can be an expensive and time-consuming process. A lot can therefore potentially be gained from exploring more effective alternative methods of track inspection. The use of Ground Penetrating Radar in transportation maintenance applications has seen an increase in the later years, and it is desirable to accurately study the extent of its abilities for this application.

Hypothesis

> Is it possible to use Ground Penetrating Radar (GPR) to detect anomalies such as ballast pockets, and distribution of water content in railway ballast?

Scope

The main goal of this thesis is to assess the abilities of Ground Penetrating Radar in the following railway applications:

- Detection of subsurface track body anomalies like ballast pockets and animal burrows.

- Mapping the distribution of water in the track body.

Initial plans to also develop a framework for automatic detection of ballast pockets were stopped due to time constraints and the discovery of similar systems already in development.

There has been very little research activity with GPR for railway in Norway in the past, and knowledge of the technology is not widespread. As a result, this thesis has been developed with the intention to also serve as a comprehensible introduction to the subject, as well as providing an updated view on the most recent advancements in relevant railway applications.

1.1   Methodology

The process consisted of a thorough literature review, and a field study conducted on live track.

Literature review

The goal of the literature review was to gather detailed information on the theoretic principles behind the GPR technology, and to assess the progress of recent studies on its applications. As such, the review included two slightly different approaches towards the material. Literature regarding the basic principles of GPR is widely available, and is largely uncontested between sources. Results from field and laboratory studies are also included here. Some of these are difficult to confirm from independent sources, but some extra merit is still given through publication in peer-reviewed journals. During the work with this thesis, some errors were still found in peer-reviewed sources, but the nature of these errors was attributed to careless mistakes from the authors (such as mixing up numbers from a separate source) rather than malicious intent.

Publications originating from organisations or corporations with obvious financial interests are handled more carefully. Information from these which can not be verified through other sources or somehow seem partial were either excluded or are identified as such in the thesis text.

Each source's year of publication was taken into consideration as the GPR technology is rapidly developing over time. Especially in regards to available hardware and data processing power. Sources describing the basic concepts of track deterioration and GPR mechanisms are less time sensitive, as these are established concepts which remain true over time.

As the field of GPR research is relatively small (especially for railway applications), some researchers are recurring contributors to the source material. This is an inevitability which has been addressed by as much as possible confirming the validity of the most frequently featured researchers.

Data was sourced through:

- The NTNU University Library

- Openly accessible online search engines (Google Scholar, ScienceDirect)

- Technical manuals for the utilised equipment

- Literature recommendations from supervisor and scientific personnel

This method of literature review was considered to be the optimal method of acquiring data, as it allowed for easy access to most of the available data while keeping track of its origins.

Field study
From the theoretical basis acquired through the literature review, a series of field tests were designed to test the GPR in real world conditions. An actual test of the equipment was deemed to be the absolute best method of confirming the GPR's surveying abilities, and to uncover any major difficulties related to the implementation of the method. The theoretical abilities of the system were tested, and all the necessary preparations were made to be able to use it on a railway track. The field study mainly consisted of two parts:

- Test survey

- Water distribution test

Performing the field study on a live track ensured a realistic testing environment, but also gave less control over the testing conditions. This resulted in the tests being affected by rainfall, and causing time window restrictions on the track due to traffic.

Analysis
The analysis of the gathered data combines the theoretical and empirical data gathered from the literary review and the field study.

While the field tests are considered a quantitative method, their interpretations are based on extensive knowledge of the underlying theoretical principles of the GPR system. The interpretations of these survey results should therefore also be considered as qualitative research.

Interpretation of field study results has been performed without bias, and solely based on the information available from the literature and field study. Extraction of in-situ core samples to confirm survey findings was regrettably not possible due to the live track testing conditions.

2   Ballast

Ballasted railway tracks use a layer of crushed granulate material - known as ballast - placed between the sleepers and the subgrade. The ballast layer must perform several important functions to maintain the geometric stability of the track body and ensure safe and reliable operation of the railway.

2.1   Purpose and characteristics

The most notable roles of the ballast are to resist vertical, lateral, and longitudinal forces, distribute the pressure from the sleepers down to manageable levels for the subgrade, assist in absorbing shocks from dynamic loads, and provide immediate draining of any water away from the rails and sleepers through the ballast.

For the ballast to be able to perform these tasks, it must maintain a series of inherent properties. The hard angular particles of high strength rocks most commonly used gives strength and internal friction to the ballast body, while simultaneously leaving sufficient void space between the particles to facilitate drainage. However, over time the ballast will start to lose its strength and void spaces. This occurs either by mechanical deterioration of the aggregate material, or through contamination by introduction of foreign materials (fines, fluids, organic material etc.) into the ballast.

The ballast body can be categorised into four zones, as done by Selig and Waters (1984):

- Crib - material between sleepers

- Shoulder - material beyond the sleeper ends down to the bottom of the ballast layer

- Top ballast - upper portion of supporting ballast layer which is disturbed by tamping

- Bottom ballast - lower portion of supporting ballast layer which is not disturbed by tamping and which generally is the more fouled portion.

2.2 Ballast deterioration and faults

The underlying causes and mechanisms which contribute to ballast deterioration and faults is an extensive subject. In this study we are focusing on a select few situations which have been known to reduce the structural properties of the ballast or track body.
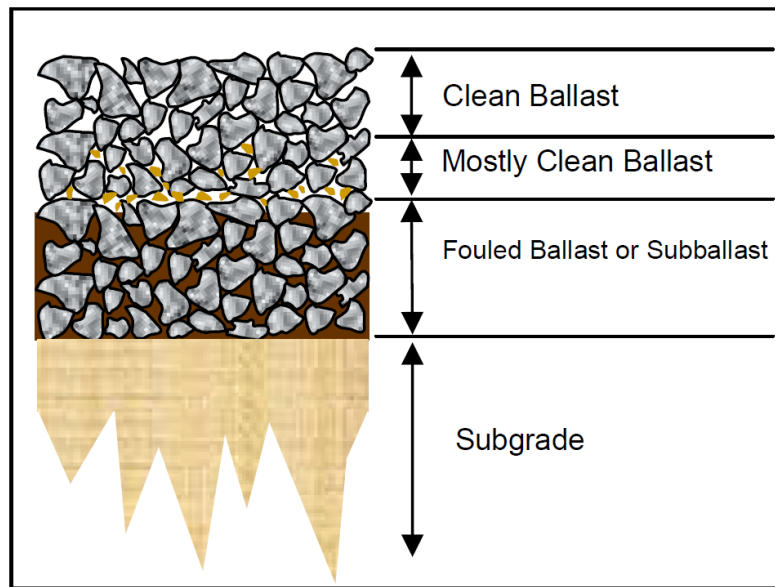
Figure 1: Varying degrees of fouling in active railroad ballast (Roberts et al., 2009)

2.2.1 Ballast fouling

Used to denote contamination by fines, ballast fouling can manifest itself in different ways, and have several different causes. It is considered the main contributor to ballast problems. (Selig and Cantrell, 2001)

Selig and Waters (1984) divided the causes of fouling into five categories, with varying contributions.

1. Ballast breakdown (76 %)

2. Infiltration from underlying granular layers (13 %)

3. Infiltration from ballast surface (7 %)

4. Subgrade infiltration (3 %)

5. Sleeper wear (1 % for wooden sleepers)

- *Ballast breakdown* comes from the repeated cyclic loading from traffic on the track (as well as some material wear from tamping, initial transport and handling), where the angular edges of the ballast material are broken off into smaller pieces. Thus, over time this process both reduces internal friction within the ballast (reducing shear strength) as well as introducing fines. (Indraratna et al., 2011)

- *Infiltration from underlying granular layers* refers to the upwards migration of fines from lower ballast-layers.

- *Infiltration from ballast surface* indicates intrusion from air- or water-borne debris, or spilled fines from passing trains (e.g. coal/ mineral ore).

- *Subgrade infiltration* occurs when the finer grains of the subgrade migrate upwards into the ballast. This process is most commonly associated with the presence of undrained water in the track body.

- *Sleeper wear* comes from the deterioration of the sleepers under cyclic loading from traffic.

In addition to filling the void spaces used for drainage, the fouling materials (especially in combination with water) have a lubricating effect on the contact interface between the angular rocks. This reduces the internal friction of the ballast, compromising its ability to distribute pressure across the subgrade. The fouling of the ballast reduces the stability of the track to a point where ballast cleaning or complete replacement must be performed to regain the desired track stability and strength.

Significant fouling and inadequate drainage of ballast can also make it more susceptible to the formation of ice-lenses and thus frost heave in sub-zero temperatures. (Silvast et al., 2010b)

2.2.2 Ballast pockets due to subgrade depressions

Under the repeated stress of passing wheel loads, fine grained or loose soils in combination with excessive moisture can cause depressions in the subgrade. A ballast pocket forms when a depression develops in the top formation or subgrade below the tracks. (Tzanakakis, 2013; Li et al., 2015) Now unable to drain properly, this depression will start to retain water, eventually filling the ballast pocket and further softening the subgrade.
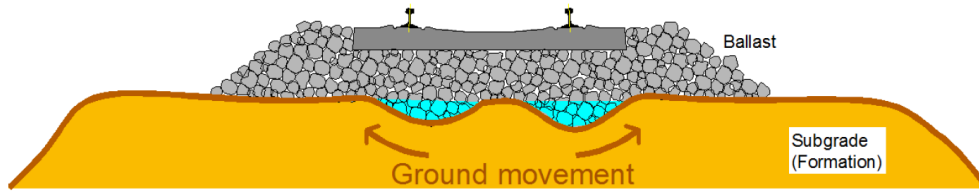
Figure 2: Early stages of ballast pocket development (Tzanakakis, 2013)

Through the cyclic loading of passing traffic, the ballast and subgrade materials will mix, fouling the ballast while further expanding the ballast pocket into the subgrade.
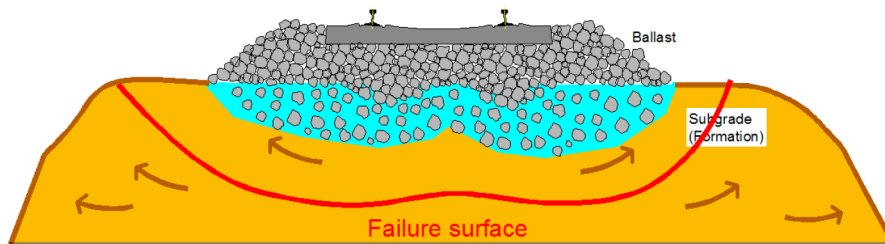
Figure 3: Further development of the ballast pocket and subgrade deterioration. (Tzanakakis, 2013)

This type of subgrade bearing failure (with shear displacement) from ballast pockets will often contribute to undesirable track geometry changes through differential track settlement. (Hay, 1982; Tzanakakis, 2013)
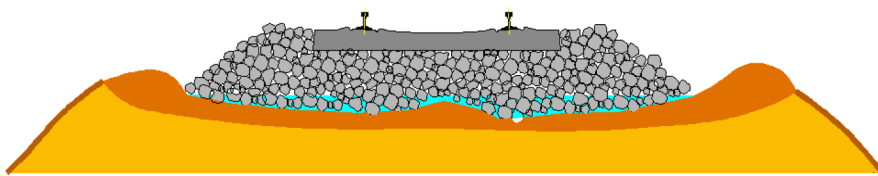
Figure 4: Highly degrated subgrade and ballast geometry. (Tzanakakis, 2013)

In addition to its detrimental effect on rolling stock, restoring track quality after such events is an extensive task, involving removal of all affected ballast and subgrade along with a regrading of the formation layer. (RailCorp Network, 2009)

If detected early, ballast pockets can be prevented from developing further by use of targeted drainage measures. Precise knowledge of the exact location and depth of the ballast pocket will allow for the most effective intervention while still avoiding large scale cleaning and renewal operations. (Hyslip et al., 2005)

2.2.3 Animal burrows

The activity of wildlife along the track presents several challenges in regards to railway operation. One such challenge comes from smaller animals burrowing dens or tunnels in the subgrade on embankments. This type of animal infestation is a regularly occurring problem in parts of the world, and may threaten the function of the track body drainage and ultimately the stability of the embankments. (RailCorp Network, 2009; Network Rail, 2010)

As these burrows mostly occur in the subgrade, they are not resolved through the normal ballast maintenance procedures (cleaning/renewal), and must therefore be met with targeted inspections and burrow-filling measures upon discovery.

2.2.4 Water/moisture retention

Without functioning drainage of the track, water will start to accumulate in the track body. The presence of trapped water in the ballast reduces its shear strength and stiffness as well as accelerating its deterioration and fouling process. (Indraratna et al., 2011)

According to Selig and Cantrell (2001), causes of restricted drainage may include:

- Ballast pocket formation from subgrade settlement

- Fouled ballast shoulder

- Low permeability boundary at edge of ballast

- Ponding of water next to the track from lack of a ditch to carry water away from the track after exiting the ballast

- Inadequate lateral slope on the subballast surface to direct water to the side of the track.

In conditions where the subgrade is largely saturated with water, even a small content of water/moisture in the interface between ballast and subgrade layer can lead to formation of a muddy slurry. As passing trains induce a cyclic loading on the track, the slurry is pumped upward, fouling the ballast through to the surface. (Selig and Waters, 1984)

Being able to detect pockets of undrained water early would allow for rectification of drainage function before the ballast deteriorates to a level that would require more extensive renewal/cleaning operations. Detailed knowledge of the water distribution will help give important information towards the causes of, and possible solutions to the drainage failure.

2.3   Current maintenance practices

To maintain and repair the tracks ballast, a method of ballast cleaning and renewal is applied. However, this is an expensive and time consuming process, disrupting train operations on the affected line. It is therefore necessary to only apply it where it is needed most, and to limit costly and less necessary use elsewhere.

The main way this is currently done is through visual inspection by railway maintenance staff, to identify potential problematic areas. (Plati et al., 2010) Samples are then excavated from these sites for evaluation of the ballast. Often these samples are taken with given intervals over a stretch of track to attempt to approximate the ballast condition of the stretch as a whole. (Hugenschmidt, 2000)

This is a destructive method of track inspection, which in addition to being time consuming, expensive, inaccurate as well as subjective in its findings, often requires interruption of regular traffic for long periods of time. (Manacorda et al., 2001; Plati et al., 2010)

There is significant potential for improvement in this process, using alternative non-destructive methods for track body and ballast inspection.

3 GPR theory and properties

Ground Penetrating Radar (GPR) is a technology that uses electromagnetic antennas, which are moved over a surface to detect reflections from subsurface features. (Annan, 2009) The concept was first attempted by El Said (1956) as a way of measuring the water table in the egyptian desert. Over the next three decades the concept found new applications like ice-thickness measurements and archeological surveys. With the rapid development in computing power starting from the late 1980s, GPR started to be seen as viable technology for an increasing number of purposes up to the wide range of applications and studies we see today. (Annan, 2003)

Figure 5: Left: Air-coupled horn-antennas. (Cassidy, 2009) Right: Air-coupled bow-tie antenna array.

Due to its ability to detect and map buried objects, GPR has seen use in many areas ranging from concrete rebar mapping to underground utilities detection. (Annan, 2003; Lalagüe, 2015) In later years GPR has started to also be seen as a viable method for inspecting roads and railways. In these applications, the use of air-coupled antennas is preferred as they are not in direct contact with the surface and can therefore survey at high speeds. This is the antenna type which will be focused on in this study. The other variant of GPR utilises a ground-coupled antenna and is used more for direct accurate imaging across smaller surfaces such as concrete slabs. (Lalagüe, 2015)

Ground Penetrating Radar can be used as a non-destructive method of surveying a stretch of track, and can be applied to achieve a continuous profile of the trackbed structure. (Plati et al., 2010) This grants significant advantages over the traditional approach of sample drillings and subjective visual inspection. GPR surveys of the track provides objective and measurable data about track bed anomalies and the ballast/ formation interface. Its utilisation enables a confident prioritisation of the maintenance programme, reducing unnecessary costs by only carrying out work where it is needed. (Gallagher et al., 1999)

Equipped with a properly shielded antenna, GPR is also able to survey track inside tunnels. (Eide et al., 2001)

The inherent properties of the GPR for revealing hidden objects/formations also make it a viable tool for detecting track deterioration anomalies at an earlier stage than with visual inspection. Thus enabling smaller pro-active maintenance measures to prevent track deterioration from developing into large and expensive track faults.

3.1 Theory

GPR surveying relies on the propagation of electromagnetic waves - and thus the magnetic and electric properties of the materials in the ground - to create an image approximation of the subsurface without disturbing the surveyed area.

At the interfaces between the the different media (e.g. ballast/subgrade, subgrade/water table), there is a contrast in dielectric constant. This difference in constants causes a portion of the signal energy to be reflected back towards the receiver and registered as voltage amplitude in relation to time. A large difference in constants give a large signal reflection and thus a large signal amplitude. (Jack and Jackson, 1999; Plati et al., 2010; Indraratna et al., 2011)

For practical GPR purposes, the most defining electromagnetic parameters for subsurface materials are the electrical conductivity σ and the dielectric permittivity ε.

3.1.1 Electrical conductivity

The electrical conductivity (σ) is a measure of free charge movement in the material and it affects the attenuation of the signal. A high value of σ in a medium will cause much of the EM-energy to be lost as heat through the conduction process. As such, surveying in media with high electrical conductivity (e.g. metals, saline solutions or clay rich environments) leads to high signal attenuation and effectively limits the signal penetration depth. These are known as "lossy" materials. (Jack and Jackson, 1999) It also weakens the strength of reflected signals, rendering the GPR largely ineffective in these environments. Signal attenuation increases with both material conductivity and antenna frequency. (Cassidy, 2009)
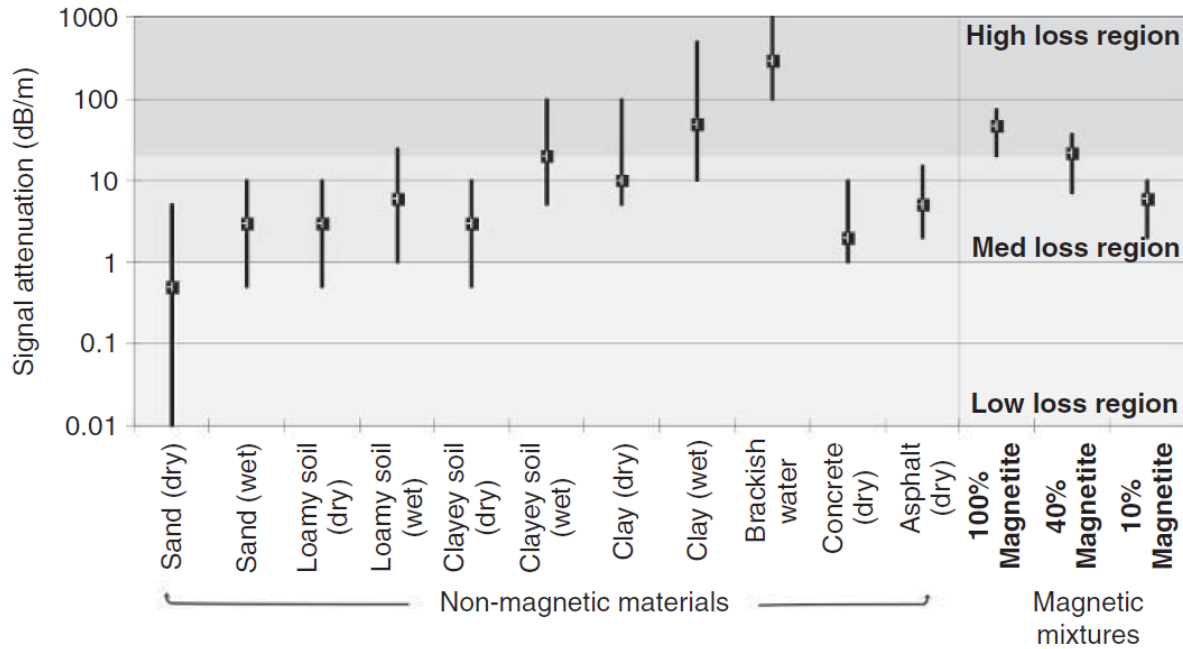
Figure 6: Typical material attenuation values and ranges for common near surface materials. (Cassidy, 2009)

The signal attenuation from the presence of free water will increase with increasing signal frequencies up to approximately 19 GHz. Although this is well beyond the frequency scope of GPR radars, the effect is noticeable already at 1-2 GHz. This means high-frequency surveys may be even more limited in penetration depth performed on certain types of wet materials. (Annan, 2003; Cassidy, 2009)

3.1.2 Dielectric permittivity

The dielectric permittivity (ε) characterises a materials ability to store and release electromagnetic energy, and it is directly linked to the velocity at which EM waves propagate through the medium. An increased permittivity will decrease the signal propagation velocity. (Cassidy, 2009) The term "dielectric constant", or relative permittivity (ε_r) is often used when describing a materials permittivity. It is defined as:

$$\varepsilon_r = \frac{\varepsilon}{\varepsilon_0} \tag{1}$$

Where:

- ε is the dielectric permittivity of the material in question

- ε_0 is the dielectric permittivity of vacuum ($8.8542 \times 10^{-12} F/m$)

(Cassidy, 2009)

The permittivity of a medium will vary greatly with the presence of water, as free water will polarise under the influence of an applied electric field and increase permittivity with an increase in water content. Where most materials commonly found in railway ballast and subgrade typically have dry permittivities of about 3-8, water has a permittivity of roughly 80. (Annan, 2009) The dielectric constant of a ballast is linearly proportional to its percentage of water content. (Fontul et al., 2014)

This effect is not as prominent for bound water, (either frozen or as surface water bonded to mineral grains) as the molecular rotation of the water is more restricted. (Grote et al., 2005) For practical purposes, frozen water can be considered a frequency-independent low-loss medium. As a result, moisture levels need to exceed a certain saturation level in grained materials (over 1 % depending on grain size) to affect overall permittivity. (Cassidy, 2009)

3.2 Analysis of survey data

> "Key to our understanding of GPR is the fact that the image we see on the screen is not a cross-section of the subsurface but is, instead, the time-dependent response of the subsurface materials to the propagation of EM energy, as recorded at the receiving antenna." (Cassidy, 2009)

To relate the y-axis unit (time) to the actual depth of the detected interfaces, we need to know the signal propagation velocity through the subsurface media. Its value will depend on the materials EM-properties, voids and moisture content. (Cassidy, 2009)
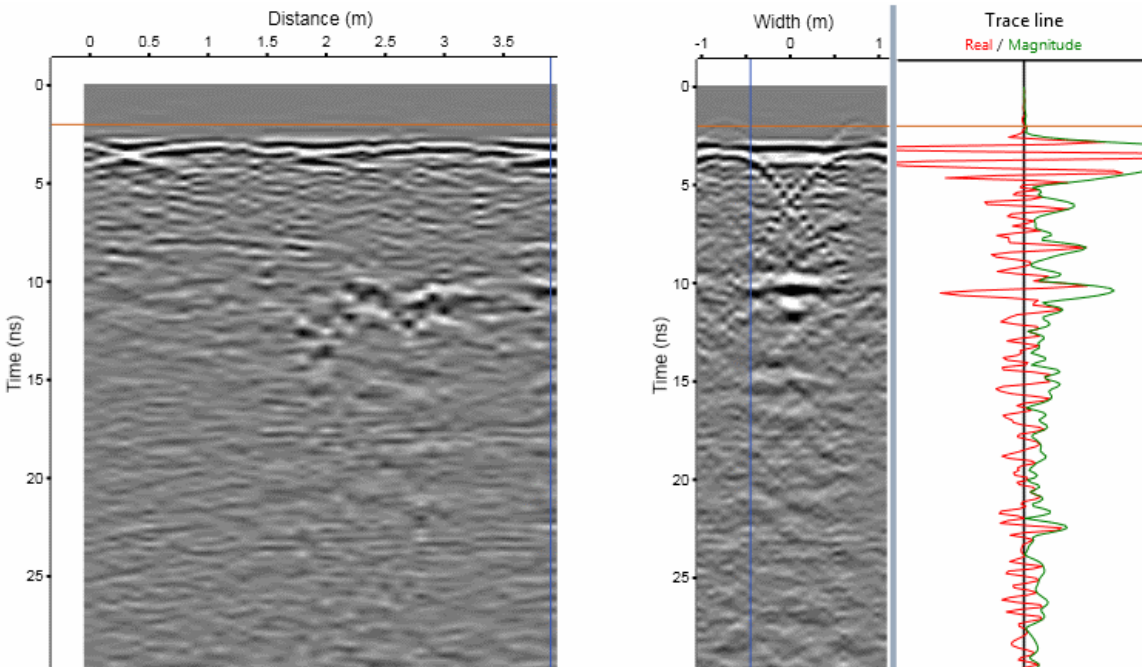
Figure 7: Example of radargram resulting from railway track survey. Left: Longitudinal profile. Right: Lateral profile and signal amplitude response.

Even when the material composition of a layer is known, the dielectric properties may not be proportional to the volume fractions of each material component. (Annan, 2009) This means there will be uncertainties in GPR measurements related to signal velocity, and numbers should be based on in-situ control testing or extensive quantitative data for similar material compositions (e.g. clean ballast with certain grade, or similarly fouled ballast).

The relative permittivity can be used to calculate the relative propagation velocity for homogeneous isotropic materials using the relation:

$$v = \frac{c}{\sqrt{\varepsilon_r}} \qquad (2)$$

Where:

- c is the propagation velocity of light in vacuum $(3 \times 10^8 m/s)$

- ε_r is the relative permittivity of the medium

(Gallagher et al., 1999; Daniels, 2004)

However, the relative permittivity will be unknown for most practical situations. (Leng and Al-Qadi, 2010)

Several studies have attempted to quantify EM wave-propagation velocities for different ballast fouling states and moisture contents. (Sussmann, 1999; Clark et al., 2001; Fontul et al., 2014)

Once the signal velocity is known or approximated, the depth of a signal reflection can be calculated using the equation:

$$d = v(\frac{t}{2}) \qquad (3)$$

Where:

- d is the depth of detected interface

- v is the signal propagation velocity through the medium

- t is the two-way travel time of the signal (Transmitter $\rightarrow$Interface reflection $\rightarrow$Receiver)

3.2.1 Signal frequency

Choice of frequency is of key importance when conducting GPR surveys. Different antenna frequencies will provoke different responses from the subsurface materials to a point where some results may only be visible in a given spectrum of frequencies.

- A higher frequency signal will not penetrate as deep as a lower range frequency signal. This is because signal attenuation increases with signal frequency. Cluttering noise also increases with increased frequencies. (Plati et al., 2010; De Bold et al., 2015)

- Poorly defined interfaces can often be more clearly imaged using lower frequencies as penetration depth is increased and noise is decreased. Around 500 MHz seems optimal for imaging the ballast/subgrade interface. (Jack and Jackson, 1999; Clark et al., 2001; Eide et al., 2001)

- 800 MHz is often considered a good choice for ballast fouling assessments. (Su et al., 2010; Shao et al., 2011)

- Higher frequencies will give better scan resolutions. (Su et al., 2010)

- Frequency also affects signal scattering from air voids in the ballast. Scattering increases with the frequency, and when the size of air voids is near the signal wavelength this can generate significant scattering of the signal. (Leng and Al-Qadi, 2010)

The frequency bandwidth of a GPR refers to the range of frequencies it can utilise in a survey. A broad bandwidth gives room to obtain both a deep signal penetration from low frequencies and the high resolution in the upper layers from the high frequencies. This optimises the sensing result. (Plati et al., 2010) However, this limits the number of scans that can be performed per second and will in practice limit the maximum surveying speed. (Annan, 2009)

3.2.2 Data processing

The raw data from a GPR profile is comprised of one-dimensional time-amplitude representations (A-scans), put together to form two dimensional representations in the distance-domain (B-scans). (Plati et al., 2010) The processing of signal data is performed to reduce noise, increase reflection contrasts and generally ease interpretation. The following are some of the main signal processing methods.
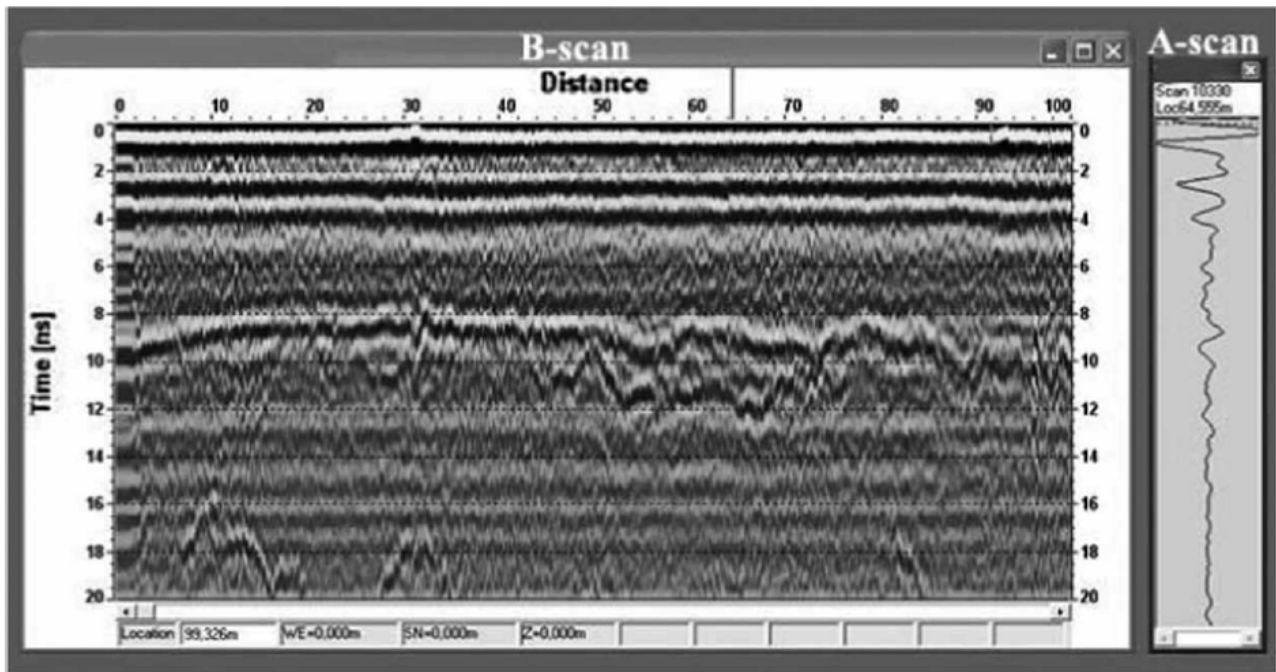
Figure 8: Typical GPR radargram. B-scan and A-scan.(Plati et al., 2010)

Time-zero correction

For air-coupled antennas, immediate signal reflection will occur at the surface interface. To avoid disturbance from these signals, time-zero corrections can be performed to adjust the earliest signal time from when the signal left the antenna, to when it first penetrated the surface. This establishes the surface as a common reference level and can also reduce the irregular reflection caused by sleepers. (Hugenschmidt, 2000)

Background removal

An unprocessed scan will display strong horizontal cluttering-bands at exact time values, often as a result of reflections from rails. Reflections from actual layer interfaces however will vary in time across the B-scan. The absolute horizontal lines seen are not representative of the actual material layering and only works to disturb the correct interpretation of layer interface data. The filtering out of "false" layering is called background removal, and helps to even out the displayed values to accentuate true layer interfaces. (Roberts et al., 2006)

Dewowing

A basic processing step where very low frequency return signals are filtered out. These low frequency signals are associated with dynamic range limitations of the instruments or inductive phenomena, known as wowing. As these signals are not objectively representative of the subsurface, but also dependent on antenna characteristics, they are usually filtered out or "dewowed". (Annan, 2003)

Filtering

Vertical band-pass filtering (only allowing a defined frequency range) is done to remove high-frequency noise and interference from the scan results. Horizontal filtering evens out the changes between A-scans to better form a unity for the B-scan. (Plati et al., 2010)

Time gain

When signals propagate through the ground, they lose energy (signal attenuation). As a result of this, reflected signals from deep interfaces are weaker than the signals from similar interfaces at shallower depths, even for identical media. To more accurately illustrate the subsurface conditions, it is possible to apply a time-dependent amplification to the signals, known as time gain or range gain. (Annan, 2009)

Inverse Q-filtering

As high signal frequencies attenuate more than lower frequency signals, a problem occurs when GPR systems simultaneously scan using multiple frequencies. Known as wavelet dispersion, it manifests on the radar scans as a characteristic blurriness that increases with depth. Inverse Q-filtering is a method for compensating for this effect. (Annan, 2009)

Topographic correction

GPR scanning is vulnerable to uneven surveying surfaces causing sudden shifts and must therefore compensate for topography in its results. Rail-mounted GPRs used on railways however, are largely unaffected by this due to the smooth nature of the rail's vertical profile. (Olhoeft and Selig, 2002; Annan, 2009)
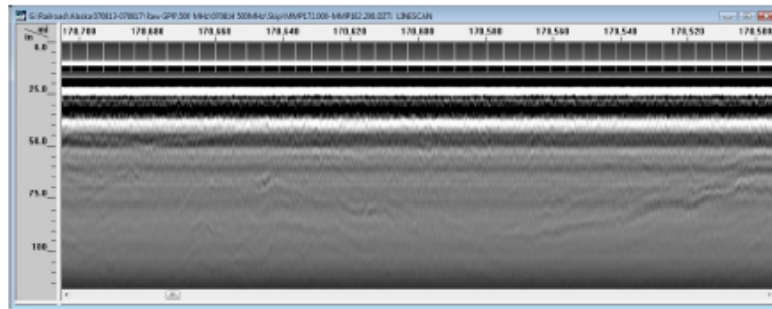
(a) Unprocessed 500 MHz data, 1 scan/ft data density
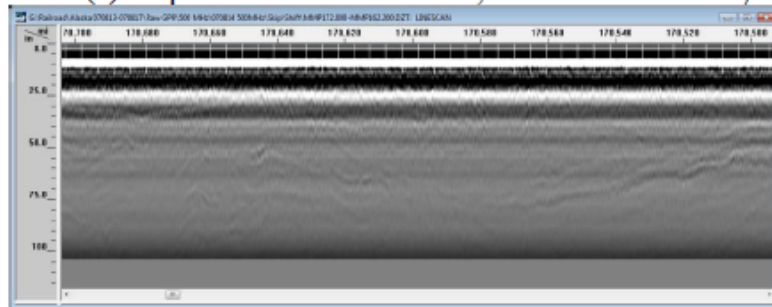
(b) Time-zero Correction
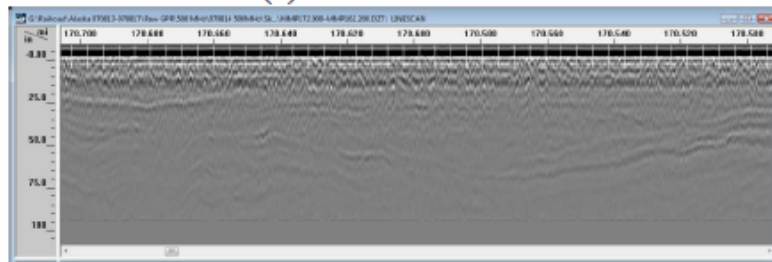
(c) Background removal
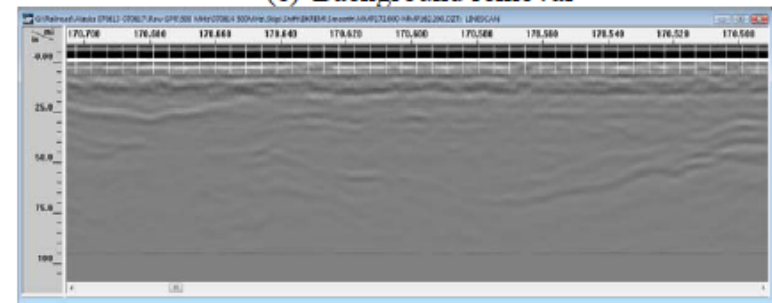
(d) Horizontal smoothing
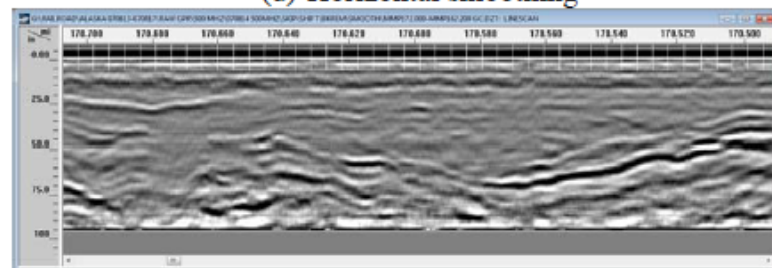
(e) 0-42 dB 2-Point Gain

Figure 9: Some common data processing steps applied to 500 MHz data.(Roberts et al., 2009)

3.3   Limitations

Although GPR technology shows promise for cost efficient and accurate ballast inspection, it does have limitations which are important to be aware of when considering it.

- The dielectric constant of ballast will vary between ballast types and must usually be approximated for field surveys. Depth- and thickness-calculations will therefore suffer some inaccuracies unless more time consuming steps (in situ measurements) are taken to verify it. (Leng and Al-Qadi, 2010)

- Ballast fouling levels will usually change gradually towards the ballast/subgrade interface. Without a clear interface with sufficient contrast in dielectric properties, it is likely the GPR will not be able to accurately locate the transition/interface. (Jack and Jackson, 1999; Leng and Al-Qadi, 2010)

- When continuously surveying active track ballast, the readings are likely to be disturbed by reflections from sleepers, rails and similar surface installations. These block the signal from penetrating through, creating a shadow directly underneath which cannot be surveyed properly. This is true for both concrete and wooden sleepers. (Gallagher et al., 1999; Hugenschmidt, 2000; Leng and Al-Qadi, 2010)

- As a medium's dielectric properties will vary both with degree of fouling and moisture content, it may be difficult to correctly attribute measured changes in value to either of the two. Surveys meant to compare a stretch of track taken at different times would therefore benefit from being performed at as similar weather conditions as possible. (Olhoeft and Selig, 2002)

- Presence of surface pollutants in the track (litter in station areas, wet leaves during autumn season etc.) may disturb GPR readings, as some of these objects produce strong signal reflections. (Hugenschmidt, 2000)

4 GPR studies and railway applications

The current high cost of track maintenance, paired with the significant potential offered by GPR technology has led to a wide range of studies on the issue. Railway track surveying is a fairly recent use for GPR, and work still remains to completely map the scope of its abilities and accuracy in this application. The following is an overview of some of the most relevant applications and studies performed on the subject

4.1 Measuring ballast layer thickness

Knowing the thickness of the track ballast layer will help maintenance personnel to assess the overall condition and performance of an active rail line. The layer needs a certain thickness to be able to distribute the loads from the sleepers across the ballast/subgrade interface, and if some areas have too thin layers, these areas will be prone to unfavorable riding conditions and accelerated ballast deterioration.

It is not uncommon for ballast layer thickness to vary along a stretch of track. Local repairs after derailments or embankment failures, varying ballast levels due to lower quality ballast or similar situations means the ballast/subgrade interface cannot be expected to remain at a level depth across the length of a track.

Several studies have been successful in determining continuous ballast layer thickness with a high degree of accuracy using GPR surveying data. (Gallagher et al., 1999; Eide et al., 2001) The clear interface reflection given by the transition between ballast and subgrade makes it possible to detect this. From the signal velocity we can calculate its depth, and thus determine the true thickness of the ballast layer. There are however some prerequisites for accurately using this method.

Clear interface

While the interface reflection from ballast/subgrade interface is usually strong, this is dependent on a high contrast in dielectric permittivity between the media. If the ballast has deteriorated, or in some way gradationally fouled near the bottom of the trackbed, (e.g. through subgrade infiltration) this will give a much less defined interface signature, and therefore make it more difficult to distinguish the exact depth of the ballast layer. (Plati et al., 2010; Fontul et al., 2014) A failure to precisely identify ballast/subgrade interface on GPR scans may therefore by itself be a sign of ballast fouling.

To make the ballast/subgrade interface more detectable with GPR, a special conductive geotextile has been developed. Placed between the two layers during the construction or ballast replacement phase, it ensures a clear electromagnetic signature at the bottom of the ballast layer. (Carpenter et al., 2004)

Accurate signal propagation velocity

Signal propagation velocity is a critical part of calculating depth, and it will vary with the dielectric properties of the surveyed medium. This is no problem for homogeneous materials with known dielectric properties, but the dielectric permittivity of ballast will vary with fouling level, void content, moisture content etc. (Leng and Al-Qadi, 2010) As a consequence, each case of ballast thickness surveying must be considered according to the current state of the ballast in question. Ballast fouling will most likely not be uniform across the depth profile of the ballast, further stressing the need for in-situ calibration.

From studies done on the subject, signal propagation velocities can be estimated for ballast based on its level of fouling. Combining the work from Clark (2001) and Sussmann (1999) gives the values in table 1.

Material (*by volume)	Source	ε_r	Velocity (m/s)
Air	(a)	1.0	3.00×10^8
Dry clean ballast	(a)	3.0	1.73×10^8
Wet clean ballast (5 % water*)	(a)	3.5	1.60×10^8
Dry clean	(b)	3.6	1.58×10^8
Dry spent	(b)	3.7	1.56×10^8
Moist clean	(b)	4.0	1.50×10^8
Dry spent ballast	(a)	4.3	1.45×10^8
Moist spent	(b)	5.1	1.32×10^8
Wet spent	(b)	7.2	1.12×10^8
Wet spent ballast (5 % water)	(a)	7.8	1.07×10^8
Saturated clean ballast	(a)	26.9	0.48×10^8
Saturated spent ballast	(a)	38.5	0.58×10^8
Water	(a)	81	0.33×10^8

Table 1: Electromagnetic properties for different ballast conditions. (a) values from Clark (2001), (b) values from Sussmann (1999). Table adapted from De Bold et al. (2015)

- The difference between the two sources for ballast in the same category ("Dry clean" has variations in value) is a testimony to the varying properties of different material types and compositions in the ballast types used. The table demonstrates the correlation fouling level and moisture content has on signal propagation velocity.

- Fouled or "spent" ballast has a higher content of fines, hence its content of voids is less than for clean ballast. As electromagnetic waves travel faster through air than through ballast material, it will also travel faster in clean ballast than in spent ballast. (De Bold et al., 2015)

- The difference between dielectric constants for "saturated clean ballast" and "saturated spent ballast" comes not only from the lower void content for spent ballast, but also from the fact that spent ballast can hold more water than clean ballast. (Clark et al., 2001; De Bold et al., 2015)

The actual properties of the surveyed ballast will most likely be somewhere between the categories seen in table 1, but they provide a good approximation for field testing. Similar values were found by Hugenschmidt (2000); Eide et al. (2001) and Fontul et al. (2014).

A relation was found by Fontul et al. (2014) where the dielectric constant increases linearly with an increase in moisture content or fouling, and fouling is the most affecting factor of the two. As the dielectric constant is affected both by moisture and fouling level, a change in its value can not be directly attributed to either of the two factors. For accurate ballast assessment it is therefore necessary to know precisely what is indicated by the GPR results. Several methods for separating the contributions of ballast density (fouling) and water content are described by Fontul et al. (2014).

Signal propagation velocity will also vary along the length of the track, as a result of local fouling, newly cleaned sections, local moisture or other factors. When operating with fixed signal propagation velocity, changes in dielectric constant along the stretch will manifest as changes in ballast thickness, even if the actual thickness remains constant. Where the signal velocity is higher than approximated, layer thickness will display as thinner, and vice versa. This is a result of the direct conversion of the signal's two-way travel time to depth from the signal velocity. If accurate ballast thickness measurement is the main purpose of a survey, in-situ calibration measurements of signal propagation velocity should be performed in relation to the uniformity of the track stretch. (Gallagher et al., 1999)

Common Midpoint test (CMP)/ Common Reflection Surface test (CRS)

For GPRs utilising a moveable antennas or multiple antennas in an array there exists a quick and accurate method for in-situ measurements of signal propagation velocity, called Common Midpoint test or Common Reflection Surface test. CMP refers to the test performed by moving a transmitter and a receiver away from each other, and CRS refers to the test performed by multiple static antennas in an array. (Su et al., 2010; Kind, 2011)

As the separation between the antennas is known, measuring a common point with multiple or movable antennas will yield data regarding differences in signal travel time. These data can then be used to calculate the signal propagation velocity in that specific point on the track stretch. (Gallagher et al., 1999; Su et al., 2010)
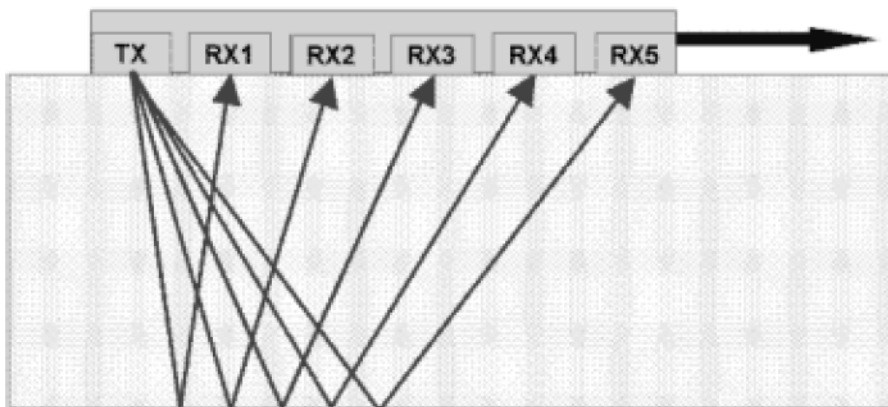
Figure 10: CRS test. Here the common reflection surface is the ballast/subgrade interface, and one transmitter sends signals received by several receivers with known relative positions. (Kind, 2011)

This method requires the presence of a clear ballast bed interface reflection and limits the surveying speed to approximately 40 km/h (for fixed antenna arrays) according to Keogh et al. (2006). If the CMP test with moving antennas is used, the surveying rig must remain stationary for the duration of the test. (Su et al., 2010) Alternatively, real layer thickness can be controlled by digging trial pits in the ballast, although this is a more intrusive and time consuming method than the CMP/CRS test. (Kind, 2011)

GPR enables ballast layer thickness measurements with high accuracy but is still reliant on in-situ calibrations and clear layer interfaces for optimal results. Changes in signal propagation velocity along a stretch of track poses certain problems for thickness

measurements, but the method is still an improvement over current methods. (Jack and Jackson, 1999)

4.2   Determining degree of ballast fouling

Accurate and updated information regarding the ballast quality on the railway network is of key importance when managing track maintenance resources. Undetected areas of poor ballast quality may over time harm both track quality and rolling stock, but ballast cleaning or renewal is an expensive and time consuming method. The more is known of the track ballast state, the easier it will be to prioritise maintenance efforts where needed most, while limiting less necessary renewals. With GPR technology there are several ways of detecting and quantifying degrees of ballast fouling.

Fouling indicated by dielectric constant
Using the same electromagnetic principles encountered when measuring ballast layer thickness, it is possible to register shifts in the dielectric constant of ballast. As the level of fouling directly affects the dielectric constant, this can help identify areas where ballast quality differs from desired values.

Surveying a stretch of track with good ballast quality, areas of poor ballast quality will register on GPR scans as areas with a thicker ballast layer. This as a result of the electromagnetic signal propagating slower through fouled ballast than in clean ballast, and thus increasing the signal travel time. It is important to note that these shifts in travel time may also come as a result of actual thicker ballast layers or local increases in water content (as water also decreases signal propagation velocity). In addition, this method does not clearly reveal boundaries of gradational fouling. As such, ballast fouling evaluation should not be based solely on the two-way travel time of the GPR signal.

Although this method is not sufficiently accurate for determining the level of ballast fouling in and of itself, it is useful for mapping the extent of "good" and "bad" ballast areas along a stretch of track. (Jack and Jackson, 1999) Shifts in ballast thickness on survey scans indicate transitions between homogeneous sections, and can then be used for targeting ballast quality investigations. (Brough et al., 2003) The absence of a clear ballast/subgrade interface may also be used as a general indicator that ballast has been at least gradationally fouled towards the bottom of the layer. (Roberts et al., 2007)

Determining ballast fouling through scattering from voids

Ballast fouling could also be assessed by taking advantage of the EM-scattering properties of ballast voids. When the wavelength of the electromagnetic signal is similar to the size of the voids, this creates significant scattering of the signal. (Leng and Al-Qadi, 2010) The air voids in clean ballast are comparable in size to the wavelength of 2 GHz signals, and therefore produce significant signal scattering when surveyed with a 2 GHz antenna. (Al-Qadi et al., 2010a) Conversely, data from fouled ballast would be expected to produce much less signal scattering, if any. (Al-Qadi et al., 2008)

Roberts et al. (2006) suggests that by using different frequencies and measuring signal scattering, it is possible to approximate the size of the voids. This can in turn be used to assess the degree of ballast fouling. A downside is that the high frequency needed (> 2 GHz) also causes high signal attenuation and therefore limits signal penetration depth.
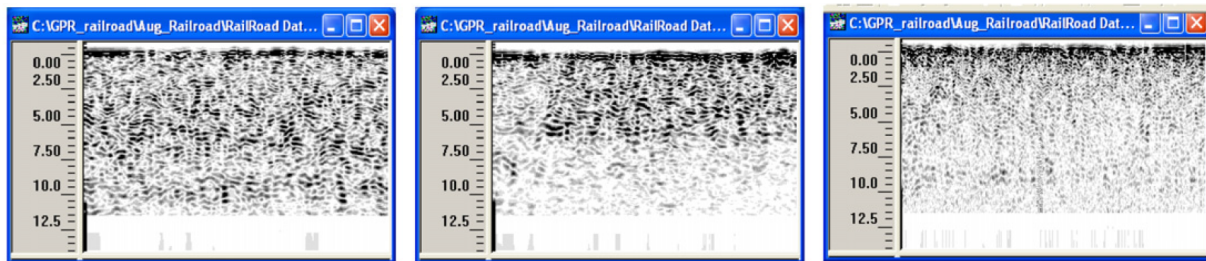
Figure 11: Scattering in radargrams with with different ballast fouling conditions. Left: Clean | Center: Partially fouled | Right: Fouled (Al-Qadi et al., 2008)

The scattering seen in the center section of fig. 11 clearly reveals the change in ballast quality occurring in the middle of the sample window. Here the ballast has deteriorated to a point where the voids no longer are large enough to cause signal scattering at the current frequency. Assuming the transition from clean to fouled ballast here is gradational (as is usually the case), lower frequency scans would not be able to identify the extent of the fouling as accurately.

To comprehensively display the scattering data, Roberts et al. (2006) uses additional data processing in what is called the "scattering amplitude envelope method". Here, changes in the amplitude of scattered signals is related to changes in ballast condition. (De Bold et al., 2015) The amplitude envelope of the reflected waves is obtained using the Hilbert transform, encompassing both negative and positive peak amplitudes. (Roberts et al., 2009) From the average scattering amplitude of signals for each depth, it is then

possible to display void content distribution (and thereby ballast quality) in the ballast layer.
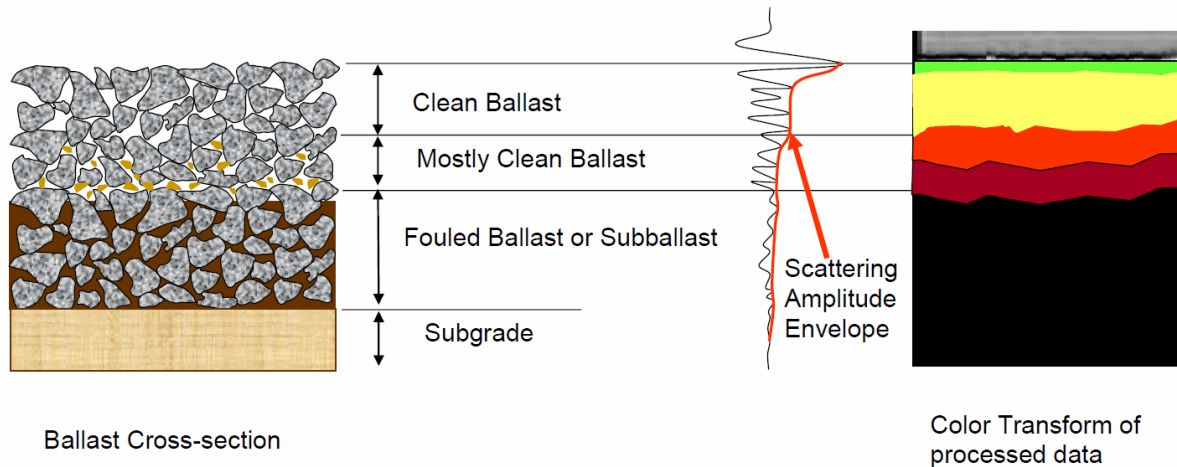
Figure 12: Scattering amplitude envelope constructed from GPR data of gradationally fouled ballast. (Roberts et al., 2009)

Practical field tests of this method has produced promising results and consistency with actual data, but more control data is needed to verify its the scope of its applicability and limitations. For one thing the method will have difficulties differentiating between the the contributions of water content and content of fouling materials. (Roberts et al., 2006; Al-Qadi et al., 2010a)

Short Time Fourier Transform(STFT)
A third approach to ballast fouling surveys with GPR is based on frequency analysis of the reflected signals, relating to the rate of signal energy attenuation through the medium. The Short Time Fourier Transform converts a portion of time-domain data to frequency-domain data, tracking the change in frequency spectrum over time, and thus over depth. (Clark et al., 2004; Oppenheim et al., 2005; Al-Qadi et al., 2010a)

The changes in frequency allows for distinguishing various ballast fouling conditions and presence of moisture, even without clearly defined interfaces. What is obtained is effectively a continuous survey of material parameters in the subsurface. (Silvast et al., 2010a)
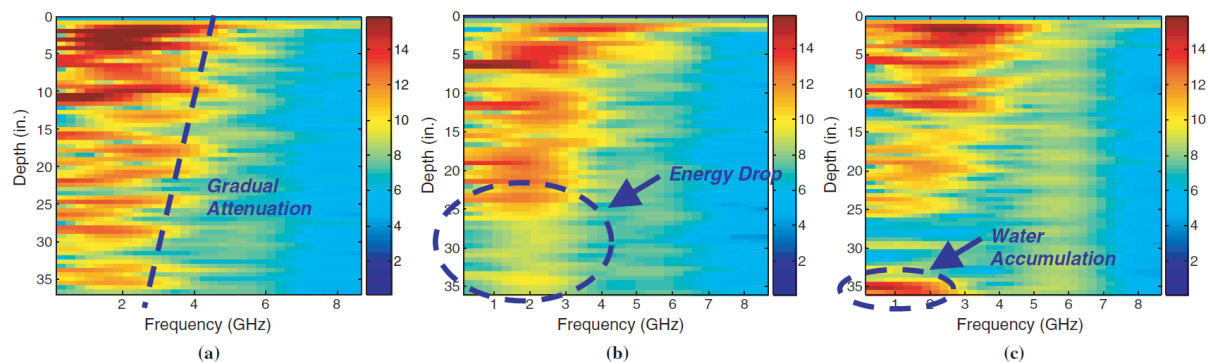
Figure 13: STFT color coding of ballast under different fouling and moisture conditions: (a) 36 inches of clean ballast, (b) 24 inches of clean ballast on top of 12 inches of 50 % fouled ballast, (c) same ballast as in b, but with added water content. (Leng and Al-Qadi, 2010)

Field and laboratory studies by Leng and Al-Qadi (2010) (see also Al-Qadi et al. (2010b)) indicate that using 2 GHz horn-antennas with STFT color-maps will enable efficient detection of fouling and water accumulation locations as long as the dielectric constant used is accurate. The automatic categorisation and color coding will enable analysis of survey data in shorter time, and limiting the need for specialised personnel. But the process will also restrict room for interpretation.

As the method will reveal information regarding ballast quality relative to depth, it may be considered superior to traditional core sample gradation tests, which only obtains data for the entire sample as a whole. (Al-Qadi et al., 2010a)

Other methods for fouling detection currently under development are not featured here, but are described further in:

- Discrete Wavelet Transform (Shangguan et al., 2012) and (Shangguan and Al-Qadi, 2014)

- System based on magnitude spectrum analysis and support vector machine (Shao et al., 2011)

4.3 Locating hidden objects/utilities

Although fouling does alter their dielectric properties, the ballast and subgrade are still relatively homogenous materials. This makes it easier to distinguish foreign objects or track related utilities on a GPR scan even in most cases of ballast fouling. (Uduwawala et al., 2005) Objects made from different materials will have different dielectric properties, and especially metals are easily detectable with GPR due to their high conductivity and strong signal reflection. (Uduwawala et al., 2005; Indraratna et al., 2011)

Plastic pipes also give unique scattered signal shapes when surveyed with GPR, but this signal is much weaker than for metals. They also become more difficult to distinguish with rising moisture levels. This is especially true for soils with high inherent permittivity. The lossy nature of the high moisture soil does not mask the signature of the plastic and metallic pipes, but does decrease the signal strength of their reflection. Their detection is therefore dependent on filtering the data by subtracting the clutter from the received signal. (Uduwawala et al., 2005)

Foreign objects will manifest with a hyperbolic inverted U-shape on the GPR response. As seen in fig. 14, the location of the object is indicated by the top of the hyperbola, and the shape of the "tails" give information regarding the signal velocity and depth. (Annan, 2003)

The antenna frequency also affects the GPR's ability to detect objects in the subsurface. Frequencies of around 1 GHz and higher increase the resolution and give finer texture radargrams. However, these frequencies generate scattering signals (noise) from voids in the ballast, which in turn make it difficult to detect layering and foreign objects. (Indraratna et al., 2011)

For optimal detection of hidden objects and utilities, lower range signal frequencies and low subsurface moisture content is preferable.
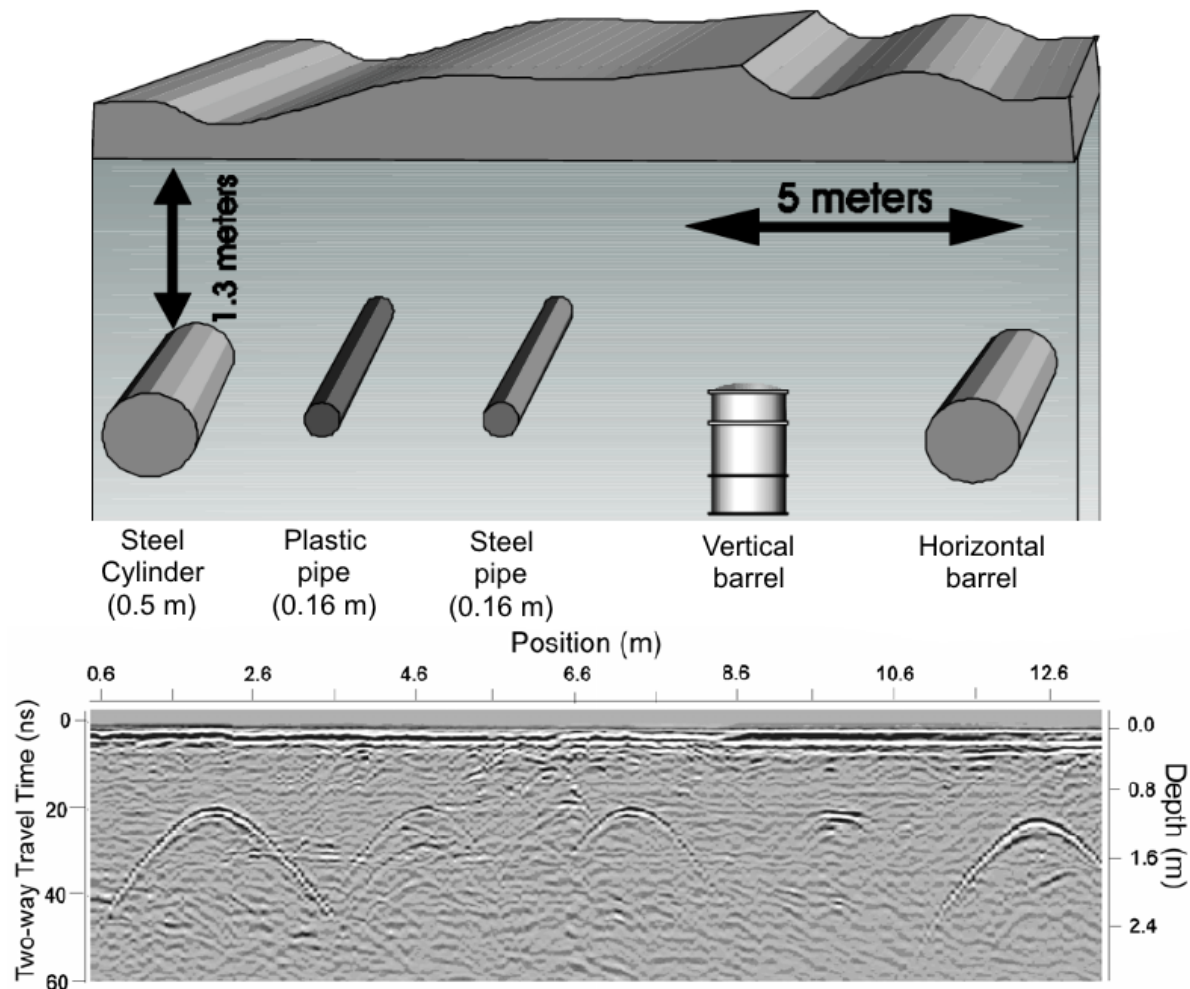
Figure 14: Buried objects detected on a 450 MHz GPR scan. (Annan, 2003)

4.4 Detecting ballast anomalies

GPR has also seen promising results as a method for detecting the presence and extent of track bed anomalies like subsoil penetration, layer deformation or mud pumping. (Hugenschmidt, 2000; Eide et al., 2001; Silvast et al., 2010b)

These types of errors will manifest on radargrams as local anomalies in the ballast bed reflection, which stand out from the common trend along the scan. Identifying these may be problematic however, as the ballast bed interface will not necessarily present itself as a straight and even line.

31

Subgrade penetration

Presence and extent of areas where subsoil has penetrated into the ballast have been reliably detected in one study by Hugenschmidt (2000). As long as the contrast to the ballast's dielectric constant is present, subgrade penetration will be visible through characteristic shapes in the ballast bed interface reflection.
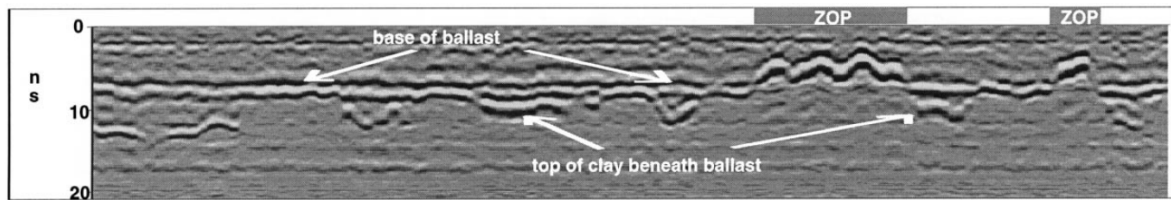
Figure 15: A 900 MHz survey dataset revealing two ZOPs (Zones of Penetration) where subgrade has penetrated up into the ballast body. (Hugenschmidt, 2000)

Ballast pockets

Ballast pockets are seen as depressions in the ballast/subgrade interface reflection, and will be distinguishable on radargrams if their magnitude makes them sufficiently stand out from the surrounding trend. The same can also be said for other trackbed anomalies like gradual slumping of the subgrade. While the benefit of early detection of ballast pockets is substantial (allowing for repair with smaller precision drainage efforts), detection will be more difficult in the early stages of development. GPR is a good method of accurately determining the depth and lowest point of ballast pockets to accurately target drainage measures. (Li et al., 2015)

Hyslip et al. (2005) demonstrates the use of generalised indices for automated systematic evaluation of substructure condition. These indices are based on the detection of the ballast/subgrade interface, and can be based on parameters like contours of layers, moisture content and the rate of change of layer parameters. This could in turn be combined with track geometry data, maintenance logs and GPS data to grant more extensive insight into track condition from only studying the available data. The development of a well calibrated index will lend substantial aid to the process of automatically detecting and classifying ballast pockets from GPR scans. Although this automatic indexing has not yet been fully developed, the work presented by Hyslip et al. (2005) is a promising proof of concept.
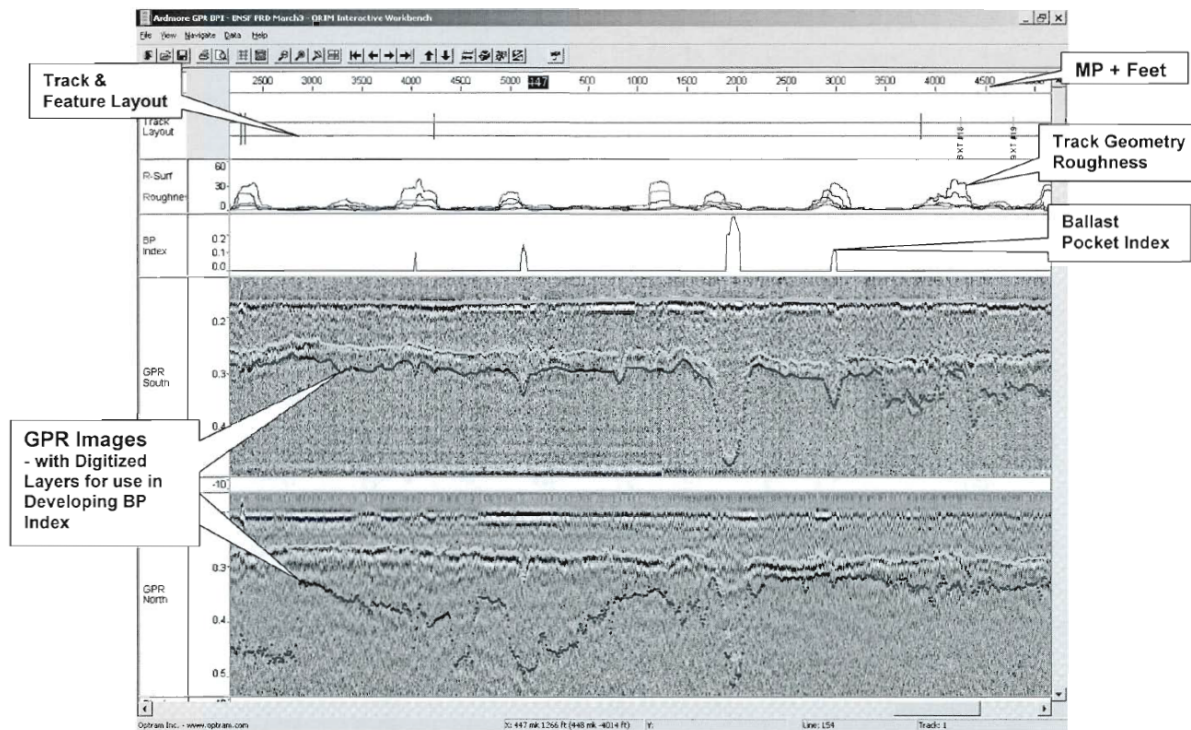
Figure 16: Automatic indexing of ballast pockets. (Hyslip et al., 2005)

Mud pumping

Mud pumping occurs when the load bearing capacity of the ballast fails, and a slurry of fines and water is pumped upwards through the ballast body by the cyclical loading of passing trains. The fines and water contribute to foul the ballast, which will in turn decrease the signal propagation velocity. Identification based on this characteristic alone may be difficult, as the upwards migration of fines from the subgrade will compromise the integrity of the ballast/subgrade interface. Thus rendering its reflected EM-signal weak or non-existent. Developing mud pumping sites may also manifest as subgrade penetration or wave-shaped reflections on GPR radargrams, before depositing fines on the surface and becoming easily detectable by visual inspection. For solutions utilising advanced signal processing for moisture or fouling detection, these areas can be identified by searching for localised areas with an increased degree of fouling. (Göbel et al., 1994)
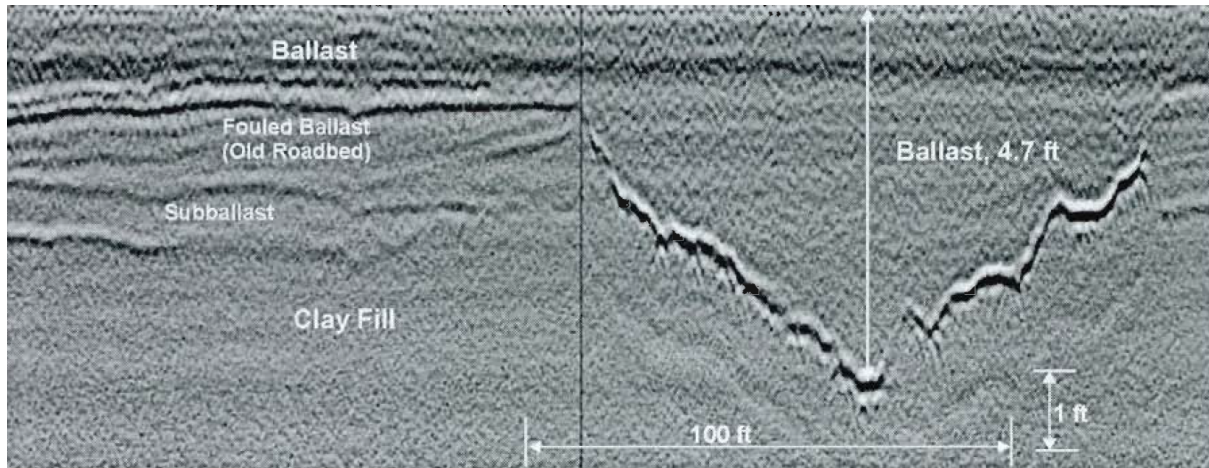
Figure 17: Deep V-shaped ballast trench. In this case an intentional drainage ditch to drain a developing ballast pocket.(Hyslip et al., 2005)

V-shapes on radargrams can be a result of ballast pockets, or deep cuts backfilled with ballast input as intentional drainage trenches to halt the further development of a ballast pocket. (Eide et al., 2001; Li et al., 2010)

4.5 Detecting frost-susceptibility and ice lens formations

For railways situated in climate zones prone to sub-zero temperatures, the freeze thaw/cycles can have a detrimental effect on track performance. This is particularly true for heavy-haul lines, as the occurrence of frost heave and thaw softening may directly affect the geometry and bearing capabilities of the track body.

For detrimental frost action to take place, three parameters must be fulfilled. In addition to temperatures below 0 °C and available moisture, the affected layer must be frost susceptible. In short this means it needs a particular composition of fines. The occurrence of such frost-susceptible material in the track structure may come from wrong use of subgrade materials or fouling from fines in the ballast layer.

Silvast et al. (2010b) performed a research project to study the potential of GPR to locate frost susceptible track sections. The approach used for detection of these situations was based both on the GPR's ability to identify frost susceptible soil (in the same way it can detect fouled ballast) and its ability to detect water.

As previously seen, water is a dominant factor in determining the dielectric properties of soils and therefore the strength of the reflected GPR signal. (Narayanan et al., 1999) However, there is a significant difference between the reflected signal strength from free water and that of bound water (e.g. frozen in ice). (Grote et al., 2005; Cassidy, 2009) As a consequence, liquid water is much easier to detect with GPR than frozen water. The detection of ice lenses performed in the Finnish study was therefore reliant on liquid water being present around the ice.

The electromagnetic signal from the GPR is reflected back towards the receiver from the interfaces between structural layers. The larger the difference in dielectric values between the two layers, the stronger the reflection becomes. Both properties necessary for frost action (water content and fines) will increase the relative permittivity and electrical conductivity of the medium, relative to clean permeable materials. This difference creates a clear and strong reflection at the interface of frost-susceptible media, thus enabling detection. (Silvast et al., 2010b)

The presence of water or fines also alters the frequency response of the GPR signal. Through the use of a STFT analysis, it is possible to differentiate between frost-susceptible and non-frost-susceptible materials (see fig. 18). This allows for more easily comprehensible color coded scan profiles for determining potential problem areas. (Silvast et al., 2010b)
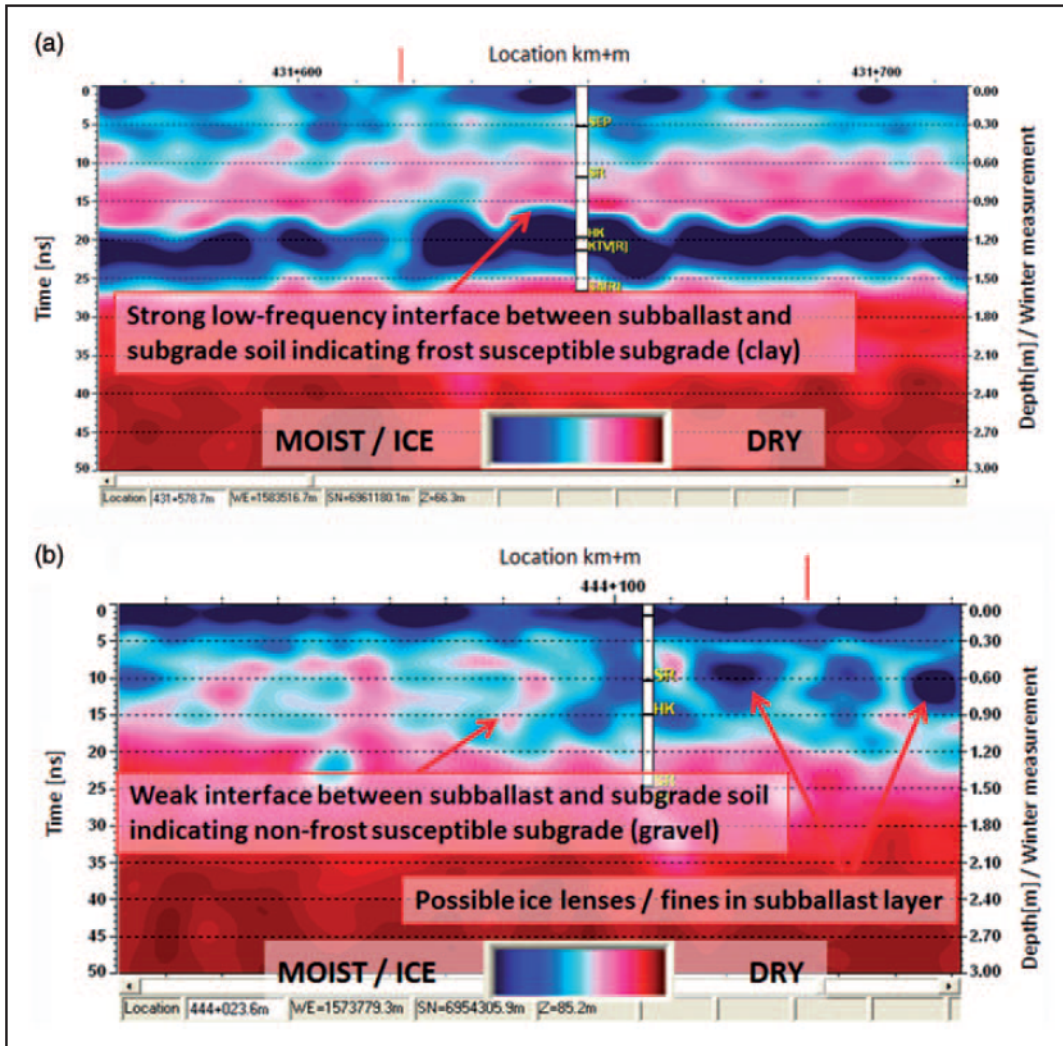
Figure 18: STFT processed GPR scans from: (a) clay subgrade, and (b) coarse gravel subgrade sections. (Silvast et al., 2010b)

In the study by Silvast et al. (2010b), GPR data allowed for estimation of frost-susceptibility by utilising the STFT analysis method and comparing data from summer and winter-surveys on the same track sections. This also allowed for ice lenses to be detected, though not with absolute accuracy and under the precondition that liquid water occurs around the ice.

4.6 Revealing water and moisture content

As the dielectric constant of water is significantly larger than both that of ballast and that of fouling materials, the presence of moisture will have a noticeable effect on GPR survey data. Surveying a section under wet conditions will yield more intense radargram textures of features than under dry conditions, especially where materials retain the moisture more than the clean permeable ballast. (Hyslip et al., 2005; Indraratna et al., 2011)

Pockets of water should also be clearly visible on GPR scans, granted they are within the signal range depth. (Narayanan et al., 1999) Experimental work with the Short Time Fourier Transform method and the amplitude envelope method have also been successful in accurate detection of water. (Al-Qadi et al., 2008; Leng and Al-Qadi, 2010)

Studies related to detection of leakage from water and sewage pipelines have found GPR to be a viable inspection method. (Ayala-Cabrera et al., 2014) Not only for detection of leaks, but also to map how water will dissipate and distribute through the soil. For optimal results, an array of antennas is needed to be able to survey the ground in three dimensions.

Work published by Su et al. (2011) and Li et al. (2015) on the "wetting test" do provide evidence of GPR's ability to detect water introduced to the ballast as a means of identifying fouled ballast. When water is detected as pooling inside the track body, it indicates poorer drainage qualities in the medium below, than above.

Though no previous study has been found to directly apply GPR specifically for mapping the water distribution in ballast, these studies at least prove the concept of some of the necessary technological functions.

5 Field study

To assess the viability of GPR systems for the applications mentioned in this thesis, a field study on live track was performed on the 27th of October, 2015. The purpose was to survey a live track section in realistic conditions, and to artificially implement track conditions and faults to assess their detectability in real situations.
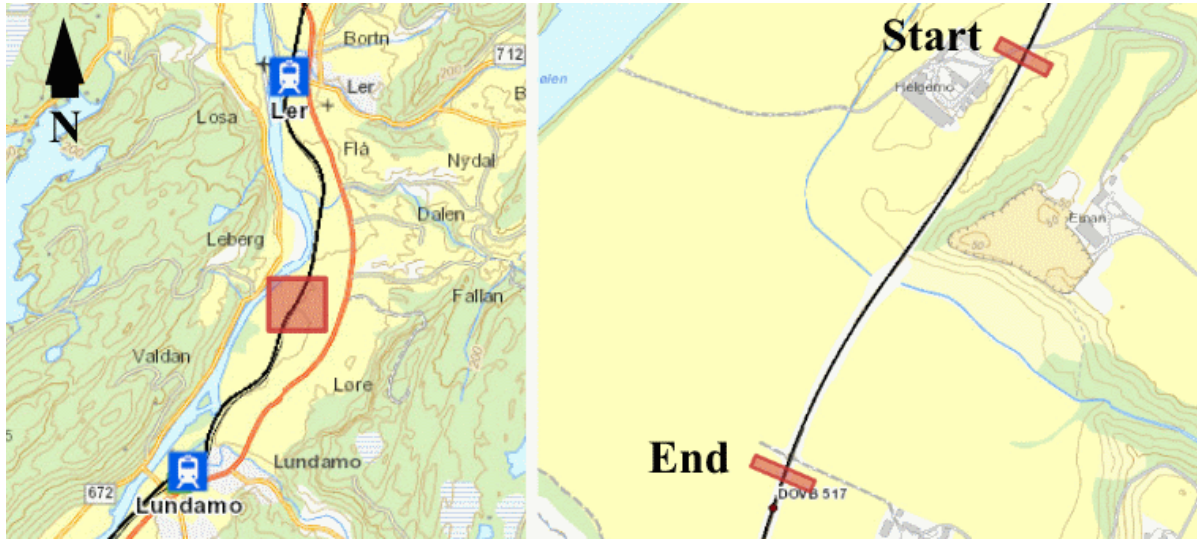
Figure 19: Track section used for test surveys. Dovrebanen 517.050 km - 517.600 km. (Jernbaneverket)

Although the initial intention was to conduct the survey on a stretch known to have ballast pockets, this was in the end not deemed feasible. Existing ballast pockets could not be reliably located, and digging operations for artificial implementation of ballast pockets were considered to be too extensive and costly for this study. Focus was instead turned towards proving the accuracy and ability of the GPR to detect the factors needed to uncover ballast pockets. A successful mapping of the ballast/subgrade interface, detection of subsurface formations and anomalies would go a long way towards proving the GPR's ability to detect the presence of ballast pockets.

The track stretch selected was a 500 m long section of Dovrebanen, situated between Ler station and Lundamo station, in Sør-Trøndelag, Norway. The section consisted of an electrified single track with concrete sleepers on ballasted track, running partially on embankments, partially on cuts and partially level to the terrain. It was selected in part as it contained several features which would provide interesting results on the GPR scans, including mud pumping sleepers and level crossings.

5.1 System description

The utilised GPR system was a GeoScope™GS3F system equipped with a V2429 antenna-array from 3d-radar AS, jointly owned by SINTEF and NTNU. The antenna was mounted to a Robel rail tractor supplied and operated by Jernbaneverket for the test.

Figure 20: 3d-radar V2429 antenna-array mounted on Robel rail-tractor

GeoScope GS3F (3GHz) - Antenna model V2429	
Frequency range	200 MHz - 3 GHz
Radar waveform	Step-frequency
Antenna width	2.4 m
Number of antenna elements/channels	29
Space between antenna elements	75 mm

Table 2: Specification data on the utilised GPR system. (3d-radar, 2009)

The antenna system consists of air-coupled bow-tie monopole pairs of receivers and transmitters. A step frequency survey approach was used, where each antenna-pair surveys in several different frequencies in steps to cover the entire bandwidth spectrum. Each A-scan then includes survey data for the entire bandwidth for each antenna element.
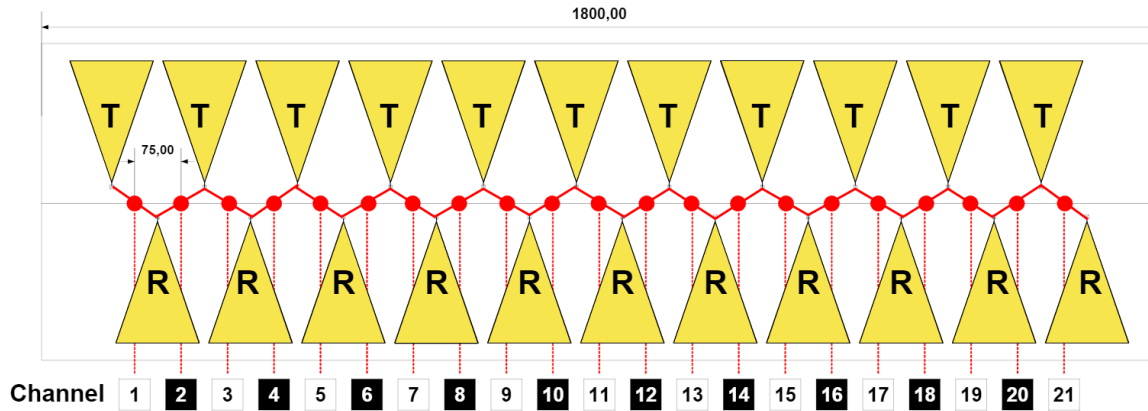
Figure 21: Antenna layout concept for similar array model with 21 antenna elements (V1821). Transmitter antennas (T) and Receiver antennas (R) are combined to create a series of elements/channels. (3d-radar, 2009)

The frequency bandwidth range utilised in the survey was 200 MHz - 2.8 GHz. This was expected to grant sufficient signal penetration depth as well as giving high-resolution scans of the upper layer textures.
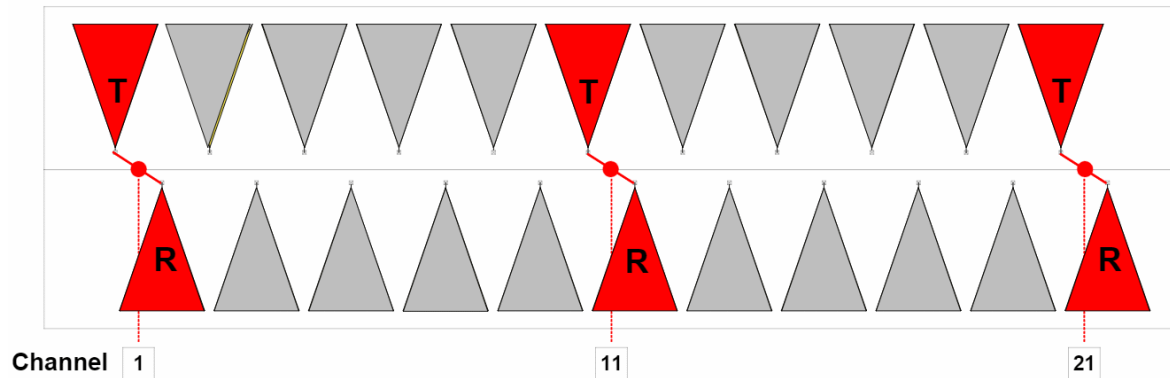
Figure 22: High-speed acquisition setup with only three active antenna pairs for V1821 model antenna array. (3d-radar, 2009)

Most of the 29 available antenna elements were used, to give best possible data for the test surveys. This did however limit the maximum surveying speed to walking pace. By using fewer of the antenna elements, the surveying speed can be increased, at a cost to

the lateral data coverage. Using only three antennas (as seen in fig. 22) will allow for surveying speeds of up to 90 km/h according to 3d-radar (2009). Successful use of the B2431 antenna model at 60 km/h was reported by Silvast et al. (2010b).

The antenna-array was mounted to a height of approximately 15 cm above the rail head. This height gives clearance to prevent antenna collisions, while simultaneously being close enough to the surface to ensure satisfactory signal conditions.

The GPR is connected to a Distance Measuring Instrument (DMI) in the form of a small rubber wheel running on top of the rail head. This wheel feeds distance information to the system to trigger scans in distance-based increments. The signal values from the wheel can be inversed from the operator PC, allowing for surveying in both directions of travel.

Figure 23: Left: The GeoScope radar unit and operator PC are located in the driver's cabin of the surveying vehicle. Right: Mounted rubber wheel (DMI)

The connected operator PC runs a GeoScope software which allows for configuring the various survey parameters like number of active antennas, frequency range or sampling intervals. During the survey it displays real-time data from one of the antennas, and can introduce markers into the dataset to correspond to surface features or other points of interest along the surveyed stretch.
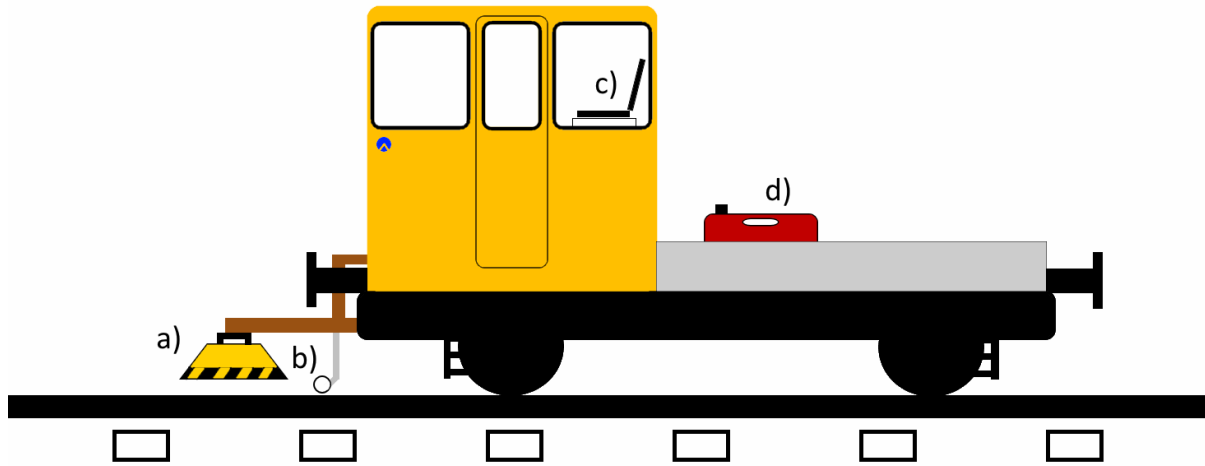
Figure 24: GPR rig schematic for the field survey. a) Antenna array, b) DMI, c) Radar unit and operator PC, d) External power source (generator).

5.2 Testing

The morning of the test surveys had seen intermediate intensity rain in the area, enough to consider the entire track body as "wet". The rain had subsided within two hours before survey start, which would have given the track time to drain itself of excess water (not bound to surface of aggregate material). Any remaining pockets of water at time of survey would then be indication of a clear failure in the track's ability to drain.

Despite the autumn season, the chosen stretch proved to be free of visible surface pollutants like wet leaves. The presence of these would most likely cause significant disturbances to the GPR readings due to the effect of moisture and biological pollutants on EM wave propagation.

Air temperature remained consistent around 5 - 7 °C for the duration of the field study.

To ensure precisely spaced scan intervals, the GPR had to be calibrated with the DMI-wheel on site. A 25 meter stretch was measured in the station area using two separate measuring systems, a measuring wheel along the rail and measuring tape. The GPR rig then ran the distance for correction of DMI length conversion factor. During this process, the rail tractor overshot the distance by approximately 0.1 m. This was however deemed within the necessary limit of accuracy, as the aim of the survey was not to precisely pinpoint features, but merely to detect and approximate their position.

Although poor signal penetration and interference from sleepers have been known to cause problems with interpretation of GPR scans, no effort was made to avoid surveying directly on top of sleepers. (Eide et al., 2001) This was an intentional decision based on a desire to keep the surveying set-up as simple as possible to operate, and instead allow any necessary signal-cleanup measures to be performed in the post-processing phase of the survey. If such a configuration proved sufficient for the test survey, it could help in limiting the technical expertise needed for the data gathering phase of future track condition inspections.

5.3 Test surveys

Procedure

The survey rig was run from the starting point to the end at an even pace. Real-time data from the GPR was displayed on the connected computer, whose operator immediately attempted to relate the revealed subsurface features to the visible surface features. This process worked to ease later off-site data interpretation, while continuously assuring the operators that the system was working as intended. For high-speed surveys over long stretches, the same effect can be achieved by combining the data with GPS-tagged photos taken in tandem with the scans.

For the first survey, the goal was mainly to confirm that the system was working as intended, and to attempt to evaluate the subsurface conditions. Surveying was stopped some distance after passing over the site of the mud pumping sleepers.

In the second survey, sampling intervals were decreased to obtain better quality of the B-scans. This increase was taxing on the system's processing power, and caused the maximum surveying speed to be limited further. The length of the surveyed stretch was increased for the second test survey to also include a level crossing with timber surface.
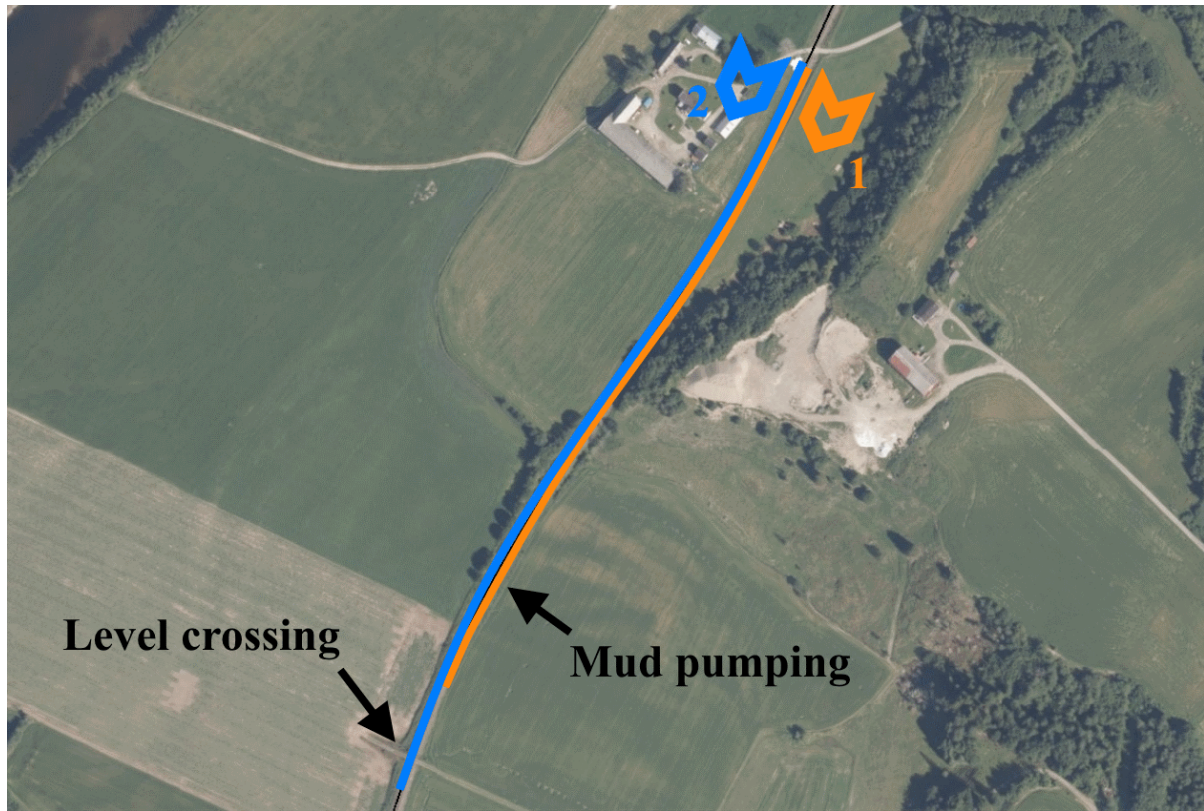
Figure 25: Extent of test survey 1 (orange) and test survey 2 (blue). Satellite image courtesy of Norge i Bilder

	Test survey 1	Test survey 2
Continuous scan between Dovrebanen profiles:	517.600 km - 517.170 km	517.600 km - 517.050 km
Survey vehicle speed:	4 km/h	3 km/h
Sample rate	1 scan every 15 cm	1 scan every 10 cm
Frequency bandwidth	200 MHz - 2.8 Ghz	200 MHz - 2.8 GHz

Table 3: Test survey specifications

5.4 Water distribution tests

Water distribution test 1 - Conditions

The first test of water distribution detection was performed at a location near the beginning of the test survey section, running approximately level to the surrounding terrain (no embankment). The ballast here appeared to be of good quality on the surface. However, shallow samples taken at the site revealed incipient light fouling in the top part of the ballast. It should therefore be assumed that the degree of fouling at that location increases somewhat towards to bottom of the ballast layer.

Figure 26: Left: Surface ballast quality. Right: Lightly fouled ballast sample excavated from the same site.

The collected ballast sample was later dried in the laboratory and found to have a water content of 0.9 % (table 4) measured in weight-percentage. This is consistent with the visual impression of the sample as very lightly fouled. The sample was taken before any additional water was introduced.

Weight of wet ballast	17.556 kg
Weight of dried ballast	17.409 kg
Ballast water content (w)	0.901832 %

Table 4: Analysis results from laboratory-dried ballast sample

Procedure

25 liters of pure liquid water was manually poured into an area at the top of the ballast (see fig. 27). It was then allowed to percolate through the ballast body while the GPR rig passed over it, scanning at recorded time-intervals. This behaviour was intended to yield information regarding the movement of the water in the lateral, longitudinal, and vertical direction as well as over time.

The water was poured solely on one side of the ballast crib to allow the data from the opposite side to serve as a control, and to confirm the GPR's ability to map the water distribution in the lateral direction. The water was not poured immediately adjacent to the rail, as signal interference from the rail could have masked the signals or otherwise complicated interpretation of the results.

Figure 27: Water being poured into the ballast at the first test site, marked in red.

A test section of 30 meters (15 meters on either side of the poured water) was set up to be surveyed for the test. This would allow for comparisons with adjacent "dry" profiles and to better emulate the image characteristics of a continuous survey. The method of surveying all 30 meters every time lead to some slight timing problems with the scan intervals. This mostly caused slight delays in the planned scanning schedule, yielding less "natural" values of time increments. However, these scans are all within the desired time area and are considered fully valid for this purpose.

A "dry" scan was performed before any water was introduced, to serve as a control against the later "wet" scans.

Water distribution test 1 - specifications

Continuous scan of stretch surrounding water pouring site	
Survey length	30 m
Survey speed	3 km/h
Sample rate	1 scan every 10 cm
Frequency bandwidth	200 MHz - 2.8 GHz
Scanning run	Time after pouring [mm:ss]
Dry run	0:00
Wet run 1	01:40
Wet run 2	03:50
Wet run 3	06:35
Wet run 4	10:35

Table 5: Specifications for water distribution test 1

Water distribution test 2 - Conditions

The second test of water distribution detection was performed at a location where mud pumping had previously been discovered, and was still clearly visible by visual inspection of the track surface. The intention was to perform the same experiment as in the first water distribution test, only altering the parameter of ballast fouling level. This part of the track runs on a small embankment.

Mud pumping is a ballast condition where fines and water form a slurry, which is pumped upwards by the cyclic loading of the track from passing traffic. This creates very localised areas where the ballast is particularly fouled, with mud filling a large share of the void spaces. The fouling will have a direct effect on the the ballasts ability to drain away excess water, and this difference should be detectable in the results of the water distribution test.
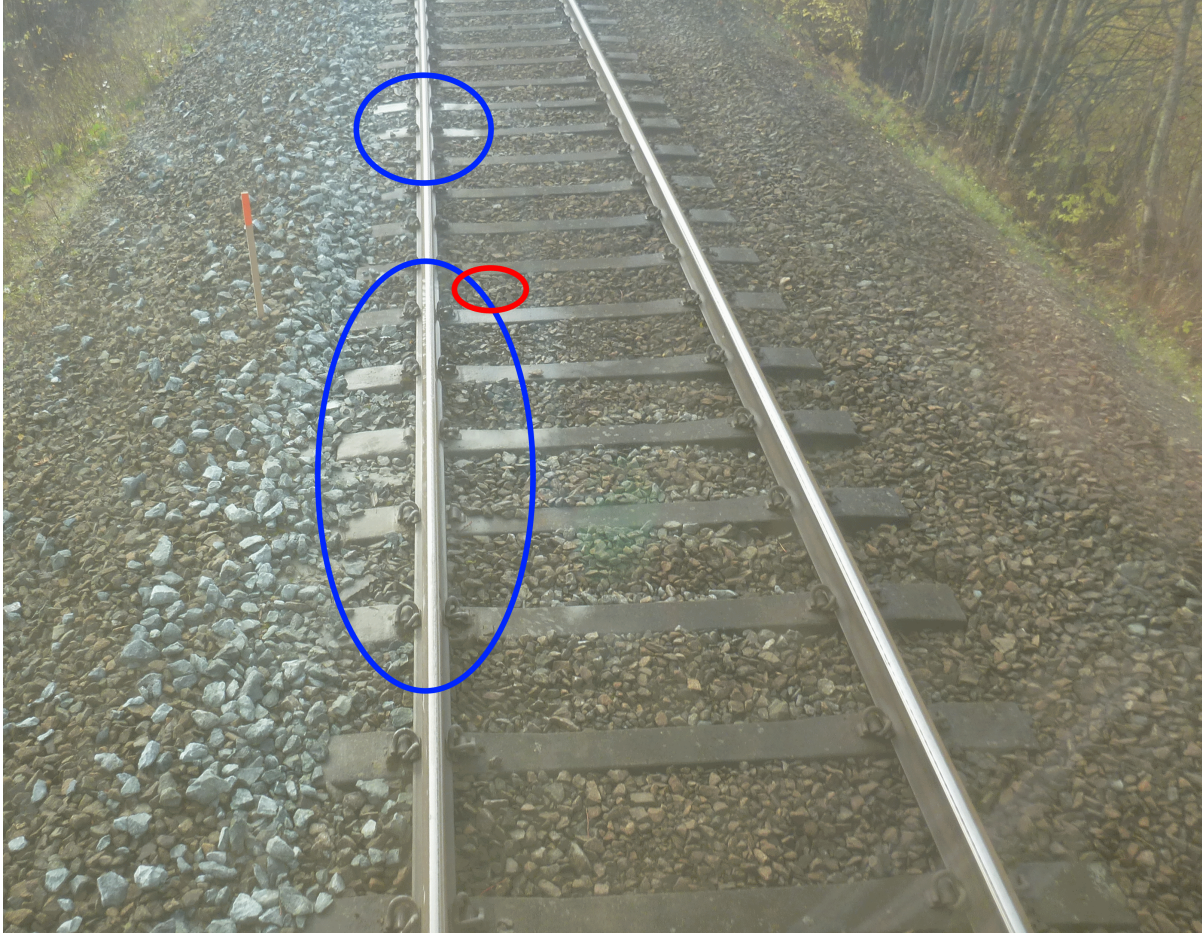
Figure 28: Blue markings indicate the extent of mud pumping sleepers at the site of the second water test. Red circle indicates the area where water was introduced into the track.

Procedure

The test was conducted with identical procedures and equipment as in the first test. 25 liters of pure liquid water was manually poured into an area at the top of the ballast (as seen in fig. 28), and allowed to percolate through the ballast body while the GPR rig passed over it.

Due to time-window restrictions on the track, there was not sufficient time to scan for the same duration of time as in the first water test. However, the time should be sufficient to expose differences in water propagation time caused by differences in ballast conditions. This also prevented the collection of ballast samples, but the general condition of the surrounding area (mud pumping) is sufficient to assume that the ballast area in question is considerably more fouled than the test area for the first water distribution test. Some

new ballast appears to have been added to the area, but not within the circled pouring area, and seemingly only on the surface.

Figure 29: Water test site 2. Fines from mud pumping clearly visible on sleeper ends and adjacent ballast. Water was poured into the area marked in red.

Water distribution test 2 - specifications

Continuous scan of stretch surrounding water pouring site	
Survey length	30 m
Survey speed	3 km/h
Sample rate	1 scan every 10 cm
Frequency bandwidth	200 MHz - 2.8 GHz
Scanning run	Time after pouring [mm:ss]
Dry run	0:00
Wet run 1	01:00
Wet run 2	02:25
Wet run 3	04:30

Table 6: Specifications for water distribution test 2

5.5 Animal burrow detection test

The initial plan for this test involved digging a very narrow passage into an embankment and surveying it with the GPR in an attempt to assess the detectability of animal burrows. However, after closer inspection of the test section, a number of problematic factors were discovered.

The embankments on the stretch were found to be slightly wider than expected, caused by shallow slope angles and deep ballast layers on the track shoulders. As a consequence, the closest and most shallow point where digging would be possible was over two meters to the side of the lateral extent of the rails, sleepers and GPR antenna array.

The compact medium, and permeating vegetation of the embankment substructure further complicated digging efforts. It was concluded that the available equipment would not allow for digging far enough into the embankment structure to approach the area directly underneath the extent of the sleepers. There were also concerns that too extensive digging might compromise the structural integrity of the embankment, making it a safety issue. The work was stopped to prioritise the other two field tests in the study.

It is difficult to predict exactly how the burrows would have manifested on the GPR radargrams, but some assumptions can be drawn from the available theory.

- While a pocket of air would present a contrast in dieletric constant (causing signal reflection), the reflection would likely be much weaker than those seen from water or metallic features. This due to the fact that the latter's dielectric constants are much larger than those of air.

- As burrows may only occur in the subgrade layer, signal attenuation will likely cause the signal to be very weak by the time it reaches those depths. This would further complicate the detection process.

- Signal reflection would likely depend on the moisture content of the surrounding subgrade and whether there is pooling of water in the burrow itself.

Future attempts to detect animal burrows with GPR should be performed on existing burrows to ensure feasibility and to provide realistic testing conditions.

6 Analysis of results

The data acquired from the field test was input into two different analysis softwares.

- Road Doctor™from Roadscanners Oy

- 3dr Examiner from 3d-radar AS

Both of these softwares provide solutions for simultaneously displaying different aspects of the GPR data, as well as built-in data processing steps to make them easier to interpret. The inclusion of both softwares was done mainly for practical reasons, as well as due to some initial technical issues with the available computers. The following data processing steps were applied to all the GPR radargrams shown in this chapter:

- Interference removal

- ISDFT (Inverse Selective Discrete Fourier Transform)

- Background removal

- Autoscale

The GPR system includes very accurate timing units which record signal travel times to within a thousandth of a nanosecond. This high degree of accuracy is useful when analysing the results of surveys, but the uncertainties related to electromagnetic properties of the surveyed medium will still give room for much larger inaccuracies in practical applications. The knowledge that these errors are unlikely to be hardware-related helps in the interpretation of survey results, and to detect methodological inaccuracies.

6.1 Test survey analysis

The GPR scans collected from the two test surveys show clear and detailed information about the track structure. From the full scan shown in fig. 30 we can begin to identify certain subsurface features. As the readability of this scan will be limited in printed version, relevant windowed excerpts have been included in the following pages.

To approximate depth values from signal travel times, a dielectric constant of 8.0 has been used for all the radargrams displayed in this chapter. From what is known of the fouling condition of the ballast in the area, this value is seemingly too high. However, as a precise wave propagation velocity was not important for the purposes of the test surveys, no further effort was taken to more accurately calibrate its value. The wave propagation velocity was more precisely calibrated for the water distribution tests.

It is important to note that the radargrams shown in the analysis part have not been fully optimised for display beyond the initial data processing methods listed in the beginning of this chapter. It is not the aim of this study to exaggerate the abilities of GPR technology, but it should still be mentioned that readability could be slightly improved using additional data processing (see fig. 9). Use of such processing steps must be done with caution, as an inherent risk of "simplifying" data is the loss of potentially important information.

The performed test survey can be seen as a realistic case study, in the sense that no information about the track was available beyond what was clearly visible on the surface. This would also be the case for a real life implementation of the method.

This chapter will mostly use data gathered from test survey 2, as it covered the longest stretch. The quality of data was very similar in the two scans, meaning that a sampling interval of 10 cm does not yield obvious advantages over an interval of 15 cm for surveying over a distance. Example radargrams with different sampling rates are shown in appendix A.

For radargrams displaying "sample" as the y-axis label, this only refers to a scaling option for the viewing software (Autoscale). While their appearance is identical to those displaying time as the y-axis unit, the sample units themselves are not directly interchangeable with time values.
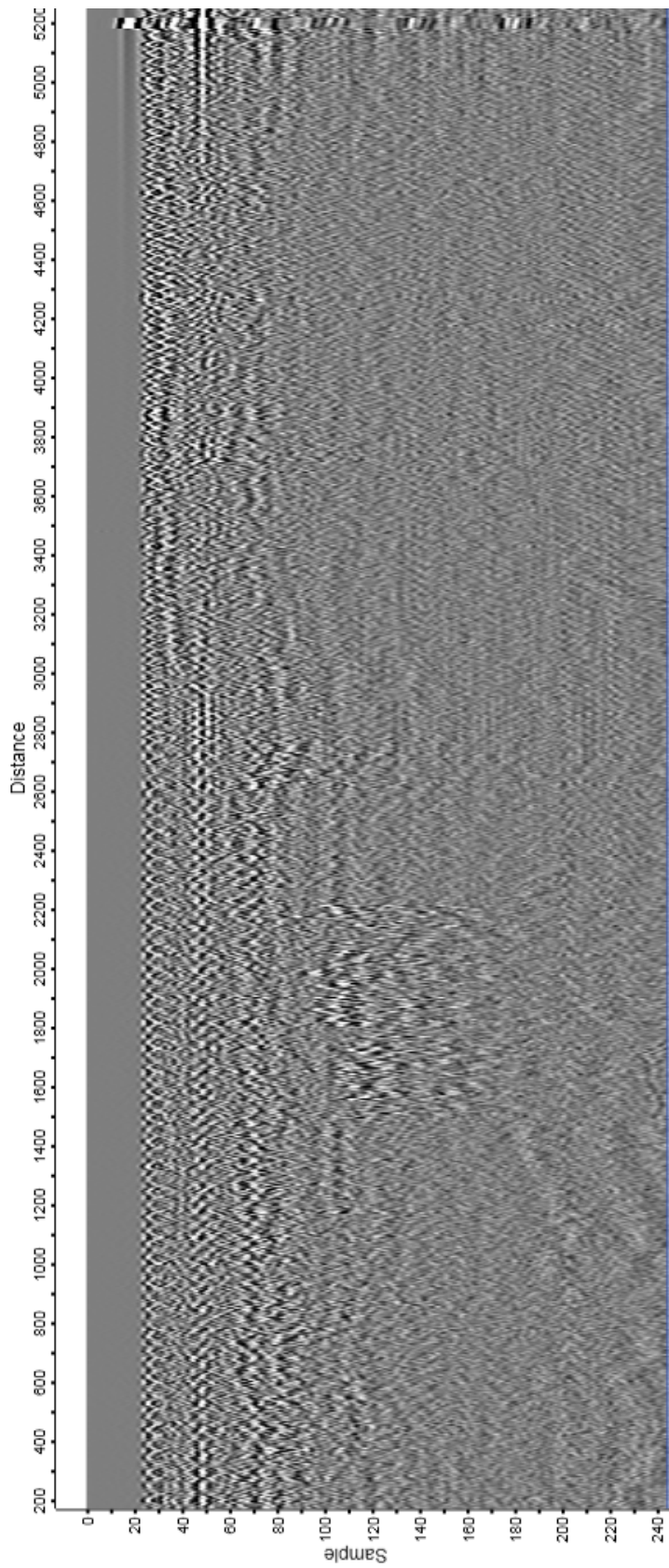
Figure 30: Full length radargram from test survey 2. Data extracted from center antenna.

6.1.1 Rock cut

A standout-feature in the survey radargram is the hyperbolic shapes occurring in the subgrade between scans 1500 - 2200. This corresponds to the section 150 m - 220 m into the survey stretch which runs in a rock cut, with a small hill directly adjacent to the line on the left side.
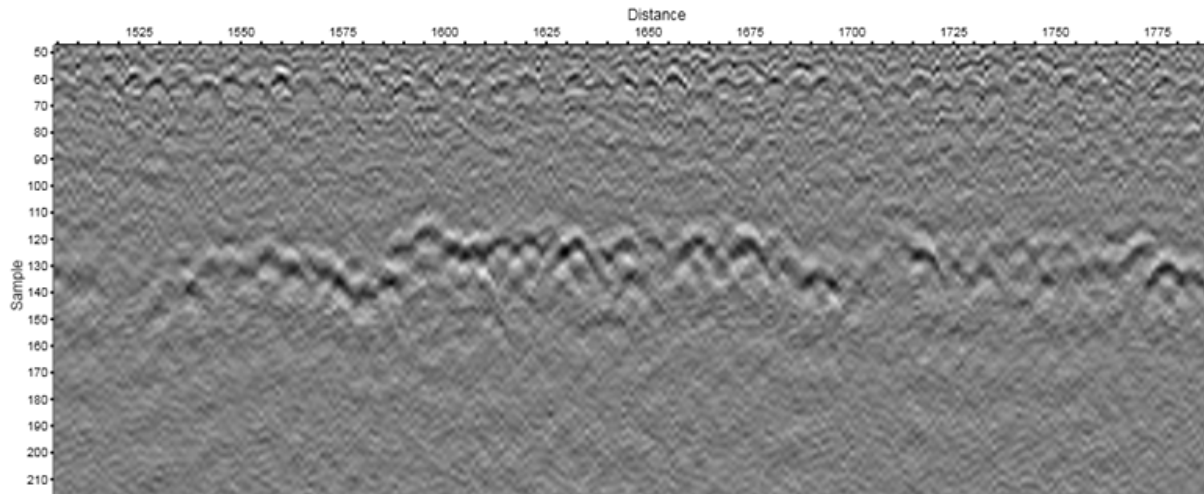
Figure 31: Clear hyperbolic shapes indicating large buried objects.
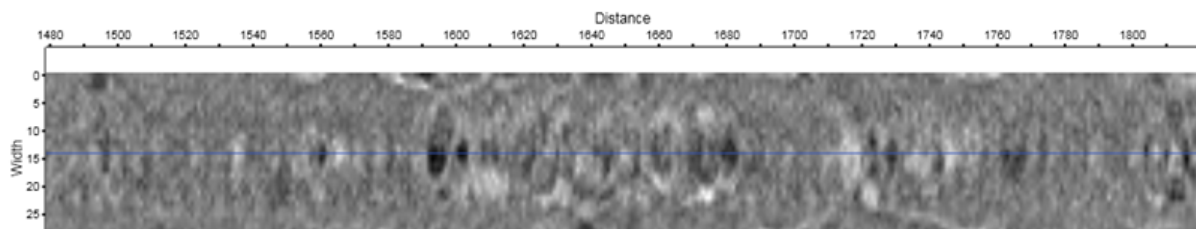
Figure 32: Horizontal cross section combining data from all antennas at the depth of the top of the hyperbolas.

The hyperbolic shapes seen in fig. 31 are most likely caused by large rocks blasted from the rock cut, and subsequently used as filler for the track body. They seem unlikely to be caused by subsurface installations due to the number of objects, apparent orientation (as indicated by hyperbola shape), and the relatively weak signal strength. Especially metallic objects would produce stronger and more distinct signals.

The horizontal cross-section seen in fig. 32 seems to indicate the stones are mostly situated in the middle of the track profile, but this could simply be a result of the signals near the edges being obstructed by the rails on the surface.

As we are able to both detect these rocks and assess their depth, it should be possible to use this method to evaluate a track for similar subsurface anomalies.

6.1.2 Mud pumping sleepers

The location of the mud pumping sleepers was already known before the survey, as they were clearly visible and distinguishable on the track surface. The challenge of the test survey was to be able to detect and separate them from the surrounding track structure.
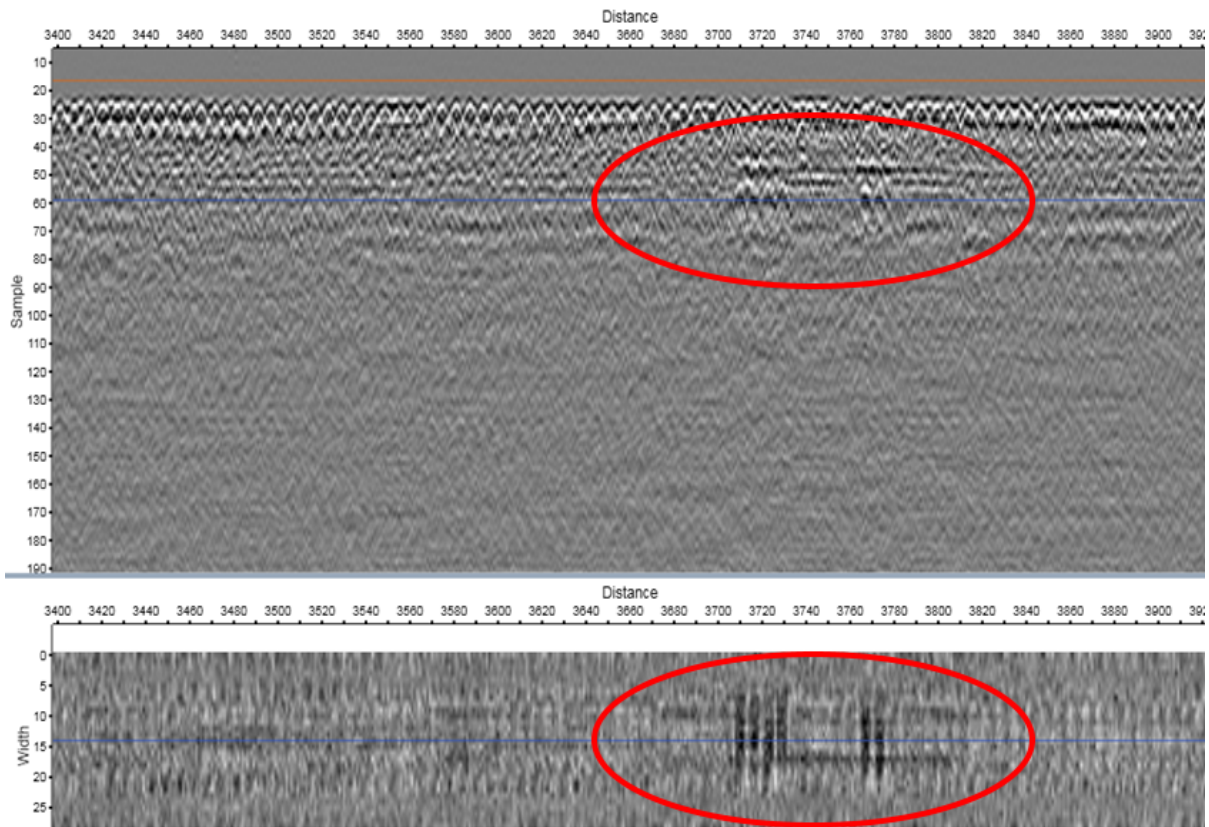
Figure 33: Mud pumping sleepers as shown on the test surveys.

The mud pumping is clearly visible on the scans in fig. 33, with clear signatures from the affected sleepers mirrored at the ballast/subgrade interface. As their reflection is mainly contained to this depth - and not continuously echoed down through the subsurface - it strengthens the credibility of the radargram manifestation. This means we can more confidently assume that the signals are a response to subgrade penetration (and not echoing from surface reflections), although in-situ excavations are needed to confirm this.

The horizontal cross-section in fig. 33 shows the signal reflection from the depth of the ballast/subgrade interface. As the shapes of the sleepers are so distinguishable at the bottom of the ballast, it is apparent that the load distribution properties of the ballast has failed more or less completely, leading forces straight down, and causing mud to be pumped up between their "footprints".

6.1.3 Signal disturbance

Displaying scans collected from antennas further from the center of the track yields a distinct and unexpected signal reflection. Further analysis of the scans reveal large shape variations in the registered reflection between the different antennas, strengthening the belief that the shape of the reflected signals did not represent the shape of any substructure feature.
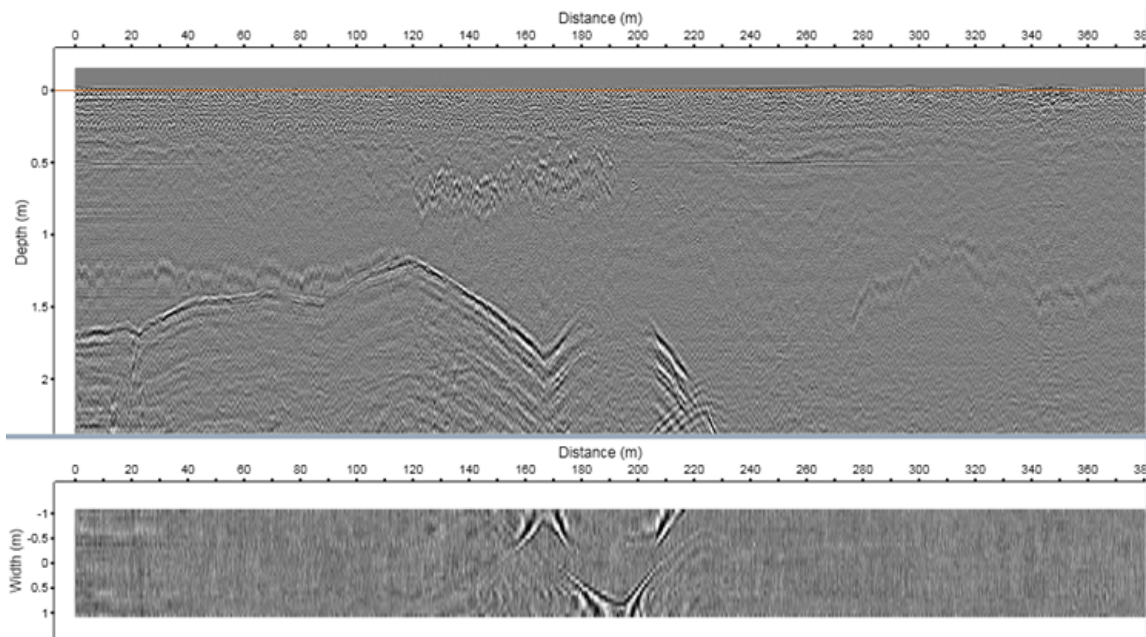
Figure 34: Strong signal reflections from deep survey depth. Top: Vertical longitudinal cross-section from left-side antenna. Bottom: Horizontal longitudinal cross-section.

From the horizontal cross section it is apparent that the strong signal reflections are originating from outside of the track body. Wave patterns are visible on both sides, but almost non-existent in the center of the survey width (0 m). Also, at these depths the signal will normally have attenuated too much to yield a strong reflection from changes in dielectric constant. When the signals here are this strong despite their apparent depth, it may be a sign that the signals have traveled in a less lossy material (e.g. air) and their depth is actually just a misinterpretation of their long signal travel time.

56

The disturbances occurred from the very beginning, until a point approximately 230 meters into the survey. Reviewing images and notes taken during the survey revealed a metal wire fence running along both sides of the track, terminating at the same point as the signal reflections. Even though the antennas only survey perpendicular to the bottom of the array, some signal scattering will still occur (this is also what causes the hyperbole shape from buried objects). In addition, the steel rails may have reflected much energy outwards to the wire fences, which was then returned and received by the antennas. This would also explain the lack of reflection registered on center antennas, as these were shielded by the rails from receiving the signal. Alternatively, the edge channels of the antenna array may not be properly shielded, and may therefore be more susceptible to signal disturbances than center channels.

The occurrence of these types of signal disturbances emphasise the importance of having a basic understanding of the theory behind the GPR scans, as blindly interpreting any radargram features as actual subsurface realities will in some cases be outright wrong.

6.1.4 Level crossings and false layering

The timber-covered level crossing located near the end of the survey stretch was easily detected on the GPR scans, and is easily identifiable by its radargram manifestation alone (fig. 35). The scans appear to reveal a vastly different subsurface structure under the level crossing than in the surrounding track, with seemingly endless layering downwards. As the substructure is no different for level crossings than for regular track, this layering is not indicative of the substructure of the crossing, but rather an unintended effect of the GPR surveying method. As the surface of the crossing is covered with timber, the signal will both experience high attenuation and give off a strong reflection. This effect is amplified by the presence of water within the timber, as was the case during this survey. The wet timber causes complete attenuation, blocking the signal completely and leaving only echoes of the initial reflection as supposed representations of subsurface reflections.

Although such "false layering" should have been removed by the applied data processing (Background removal), the longitudinal extent of the layering was in this case too short for the software to detect as surface reflection echoes. This minimum value can be manually adjusted if desired.
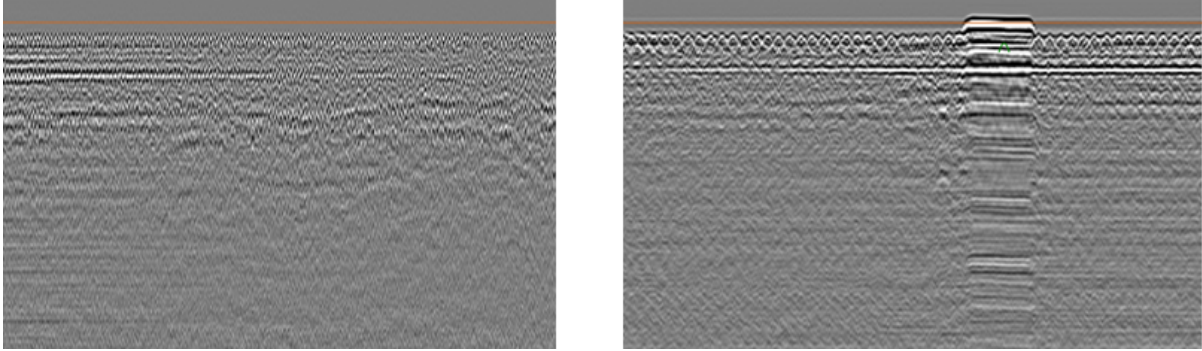
Figure 35: Left: Horizontal reflection stemming from a level crossing immediately ahead of the survey start. Right: Level crossing as manifested on the test survey radargram, with similar horizontal reflection extending to both sides, and a false layering effect downwards through the track body.

Both the radargrams in fig. 35 display a horizontal reflection extending from the level crossings (approx. 40 m), and fading away outwards from them. These are not part of the track structure, and the effect cannot immediately be attributed to errors caused by the electromagnetic mechanisms of the GPR. The most likely cause of these reflections is pooling of water in the area around the crossings.

The ballast surrounding level crossings will often be more fouled than elsewhere on the track, both due to additional ballast and timber deterioration from loading, and from spillage of fines and gravel. This would explain why this only occurs near level crossings and then fades out. The crossing roads are gravel roads trafficked mainly by a local farm with cars and assorted agricultural machinery. Although some spillage may be expected from these vehicles, the amount of traffic does not seem sufficient to cause this grade of fouling by itself.

The reflections occur at a depth approximately half way through the ballast layer. To cause such distinct reflections from water pooling, the lower half of the ballast must be nearly impermeable, indicating heavy fouling in that particular area. If the fouling was indeed caused by spillage from the road, it would be natural to assume the fouling to also appear similarly strong in the upper half of the ballast instead of this clear interface. The track is level at the site, and the road slopes away from the track on both sides, lending no aid to explaining why the water would accumulate near the crossing.

The evidence for water accumulation as the cause is therefore inconclusive, and system error cannot be ruled out without core sampling or excavation of the site.

58

6.1.5 Detecting ballast/subgrade interface

A major part of the test survey was also to attempt to detect and map the reflection from the interface between the ballast layer and the subgrade layer. From the surface samples collected as part of the water distribution test, the ballast quality is believed to be lightly fouled.

The image presented on the radargrams in fig. 36 show a definite horizontal reflection, indicative of the contrast in dielectric constant from the ballast/subgrade interface. The reflection signal is not as strong as what might be expected from clean ballast, further supporting the belief that ballast has become more fouled near the bottom of the layer. Nevertheless a definite reflection from the interface still means there is a sudden change in dielectric constant between the materials, meaning the ballast is not heavily fouled in any case.
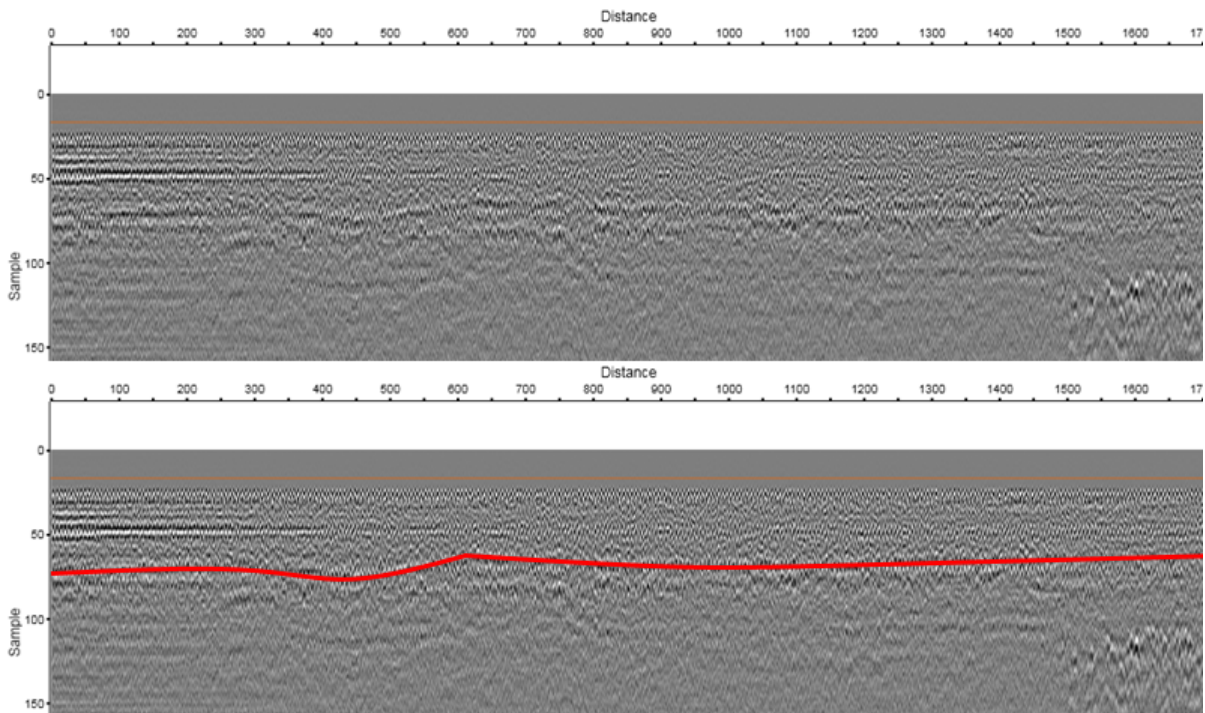
Figure 36: Top: The interface between ballast and subgrade layers as seen on the test survey scans. Bottom: The same image overlaid with a red line to aid interpretation.

From what is known about the behaviour of EM-waves in ballast, it should be possible to more accurately assess the fouling condition from high-frequency wave scattering. The implementation of this method was not possible in this thesis. However, as the utilised hardware is capable of generating the high frequencies needed, it could potentially be

included as part of future survey methods. This could yield more accurate information regarding the extent and distribution of fouling within the ballast.

When inspecting the reflection from this interface across the extent of the survey, it appears to be relatively even in depth, without sudden shifts in depth or reflection strength. This is indicative of a fairly uniform ballast composition and fouling state along the length of the surveyed section.

The successful detection of the ballast/subgrade interface means that anomalies that would cause uneven layer formation, (such as ballast pockets) would be detectable from a study of the ballast/subgrade interface reflection. In the case of this survey, the interface is so level that even small anomalies stand out from their surroundings. As ballast pockets begin to develop, they may at first not be visible across all antennas. A thorough inspection will therefore entail studying a stretch of track with comparisons between signals from antennas with different lateral positions. This way it is possible to detect early stages of localised subgrade failure.

6.1.6 Remarks

As it was not possible to extract core samples or otherwise confirm the findings from the survey in situ (beyond what was clearly visible on the surface), there will remain some uncertainty connected to the findings. Nevertheless all the detected features have plausible explanations and their extent correlates well with surface features, all but confirming their existence.

From the amount of detected features it is clear that even with fairly simple setup and data processing methods it is still possible to detect a number of anomalies and features in the track body.

Water remained in the track body from the previous rainfall, so some of the features have likely been accentuated due to local water retention, thus aiding their detectability.

With the exception of the signal disturbances seen from the wire fences, no features depended on data from all channels to be accurately detected. Coupled with the minuscule difference in data quality between the two sampling rates, it seems clear that these surveys can be performed at much higher speed without appreciable data loss.
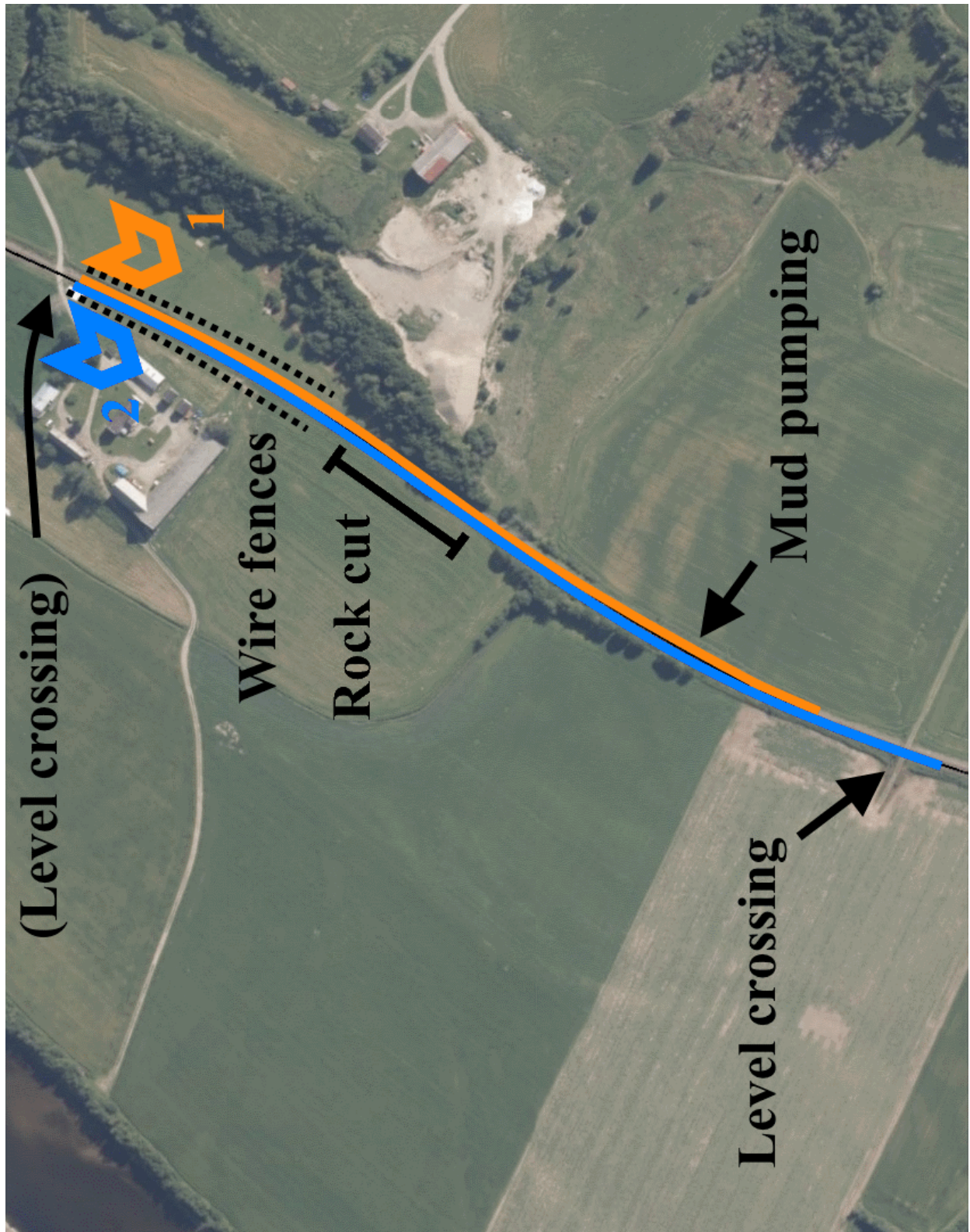
Figure 37: Location of features from the test surveys. Test survey 1 (orange) and test survey 2 (blue). Satellite image courtesy of Norge i Bilder

6.2 Water distribution test analysis

The water distribution data were analysed by carefully examining the peak amplitudes of reflected signals over the exact position of the poured water. Each run yielded signal amplitude data which was compared between runs to attempt to detect how the water was percolating through the ballast and subgrade. As the presence of water, or an increase in the amount of water will also increase the dielectric constant of the material, it will result in a stronger reflection signal. This is seen as an increase in amplitude on the GPR A-scan, where the signal's return time will indicate the depth of the water.

The process of registering amplitudes was performed manually, within the viewing tool of the Road Doctor software. Each visible peak in amplitude was inspected, with magnitude and corresponding signal travel time registered from the info given by the software. The absolute accuracy of timing the peaks can therefore not be guaranteed, but much care was taken to ensure a correct reading.

6.2.1 Water distribution test 1

For the first water distribution test, readings were collected for three different locations along the track test area (see fig. 38). The purpose of this was to establish a control test of unaffected areas to determine how large variations in results would be from an unaffected site (c) and compare them to the results from the water pouring site (a). Site (b) would work similar to the control site (c), but some change would be expected in the deeper layers, as water from site (a) would likely distribute outwards as it percolated down through the ballast and subgrade.
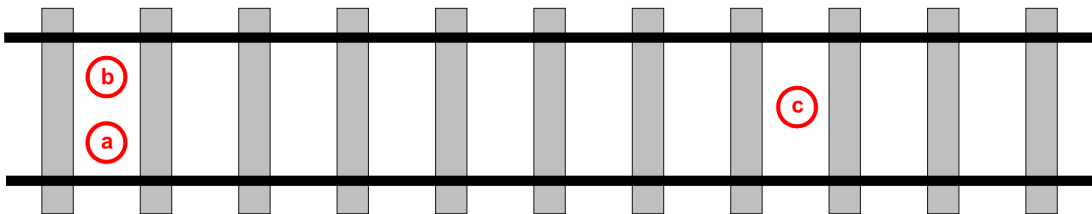

Figure 38: Location of readings collected from the area of water distribution test 1. a) Water pouring site. b) Dry side of the same ballast crib as (a). c) Unaffected control site.

To prove that the GPR is in fact able to map the distribution of water, the findings must be able to clearly detect changes in return signal strength between scanning runs. It

must be possible to accurately locate these changes in each spatial domain and the development of these changes must correlate with the assumed movement of water through the track body.

No discerning differences were observed between dry and wet B-scan radargrams from the test. This was not surprising as the track body was already very wet from the rain, and the introduced water would not have made a significant visual difference. A test performed on completely dry tracks may show differences between dry and wet scans where the reflections of certain interfaces will be accentuated due to water accumulation. In this case, a closer study of the reflected signal amplitude was necessary to differentiate scan results.
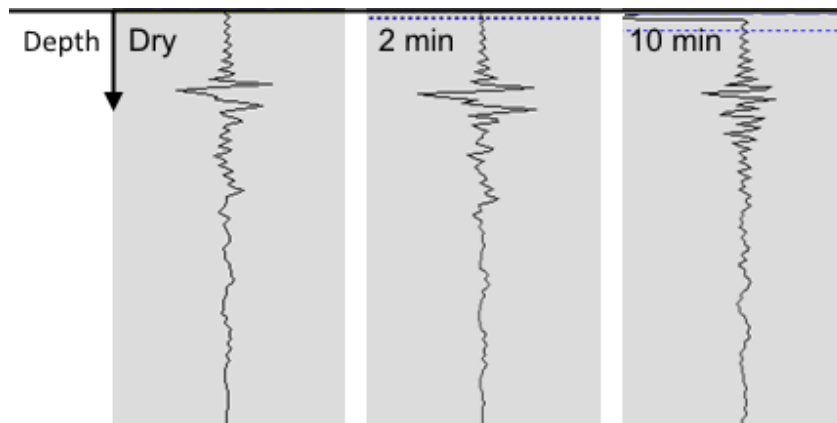
Figure 39: Reflection signal amplitude through the medium at various approximated times after water was poured. Site (a), water distribution test 1. (Image meant for illustration of result. Accuracy of scaling not absolute.)

The amplitude development in fig. 39 illustrates the direct effect from the water being introduced into the ballast.

- The dry signal is characterised by a strong initial signal reflection stemming from the signal's first contact with the surface. Amplitude then moderates through the ballast layer before slightly subsiding at what is believed to be the subgrade.

- The signal from 2 minutes after pouring does appear very similar to the dry run, but is also slightly stronger in the ballast section of the subsurface. Subgrade amplitudes appear mostly similar.

- After 10 minutes, the effects of the water are seen more clearly. Peaks in the upper parts are distributed over a wider range of depths, and larger amplitudes are seen in the subgrade.

Water distribution test 1		Channel: 22		Water test, right side (a)					
Time after pouring [mm:ss]:		01:40		03:50		06:35		10:35	
Dry		Wet run 1		Wet run 2		Wet run 3		Wet run 4	
Amplitude	Time [ns]	Amplitude	Time [ns]	Amplitude	Time [ns]	Amplitude	Time [ns]	Amplitude	Time [ns]
2432	3.052	2027	3.052	1757	3.052	2615	3.052	2029	3.052
650	4.150	1649	4.272	2104	3.784	1210	3.784	2637	3.784
669	5.737	525	5.737	1079	4.272	1317	4.272	1198	4.517
897	7.202	275	9.277	921	4.639	594	5.005	611	7.202
322	10.498	345	12.451	386	7.202	468	7.568	431	9.033
246	12.451			567	9.033	321	9.033	620	10.498
				84	10.498	659	10.498	518	12.451
				314	12.451	460	12.573		

Table 7: Time and amplitude values for water distribution test 1, site (a)

A closer look at the amplitude and time values for the water given in table 7 reveals the water distribution more accurately. As the included time values are dictated by the times at which amplitude peaks were recorded, most of them are not identical between the individual runs. Since the water affected the reflected signal amplitude, the amplitude peak times were affected by the movement of the water between scanning runs. This can initially make it difficult to discern any pattern from the numbers alone. The introduction of water should in itself alter the dielectric properties of the medium, and alter the signal travel time slightly. The reason why some runs still register exactly similar travel times is due to a slight simplification inherent in the manual registering interface. However, the magnitude of these errors is very small, and is considered negligible for this test.
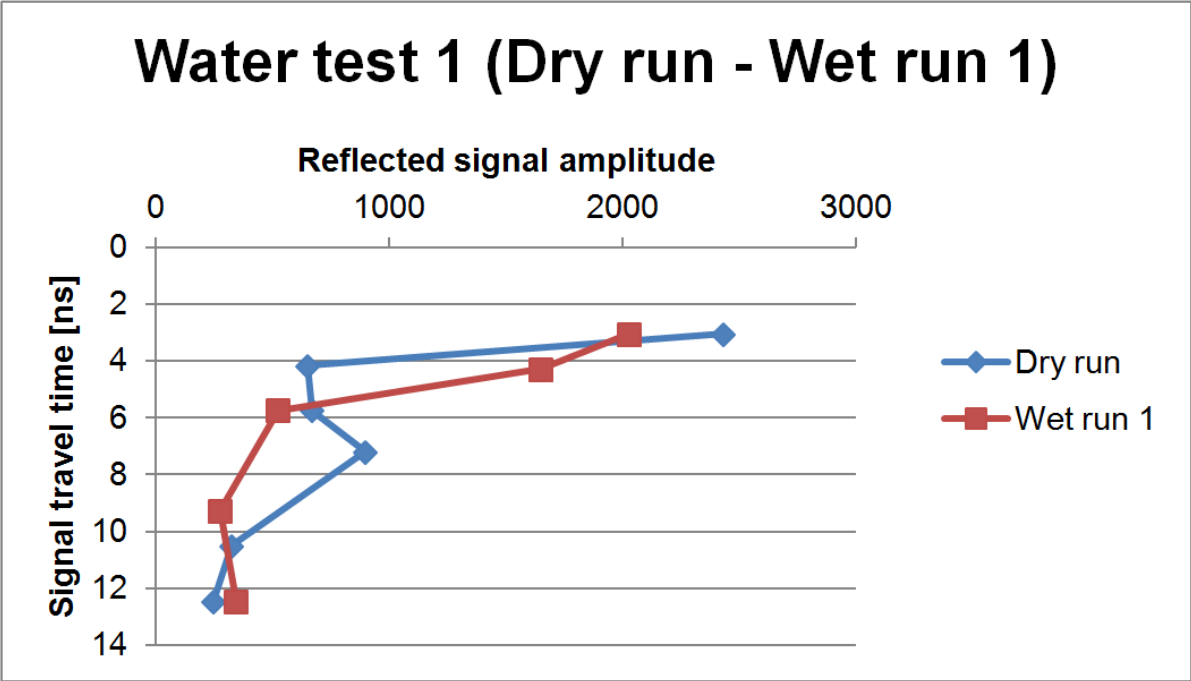
Figure 40: Amplitude time-distribution from dry run to first wet run, 01:40 minutes after water pouring.
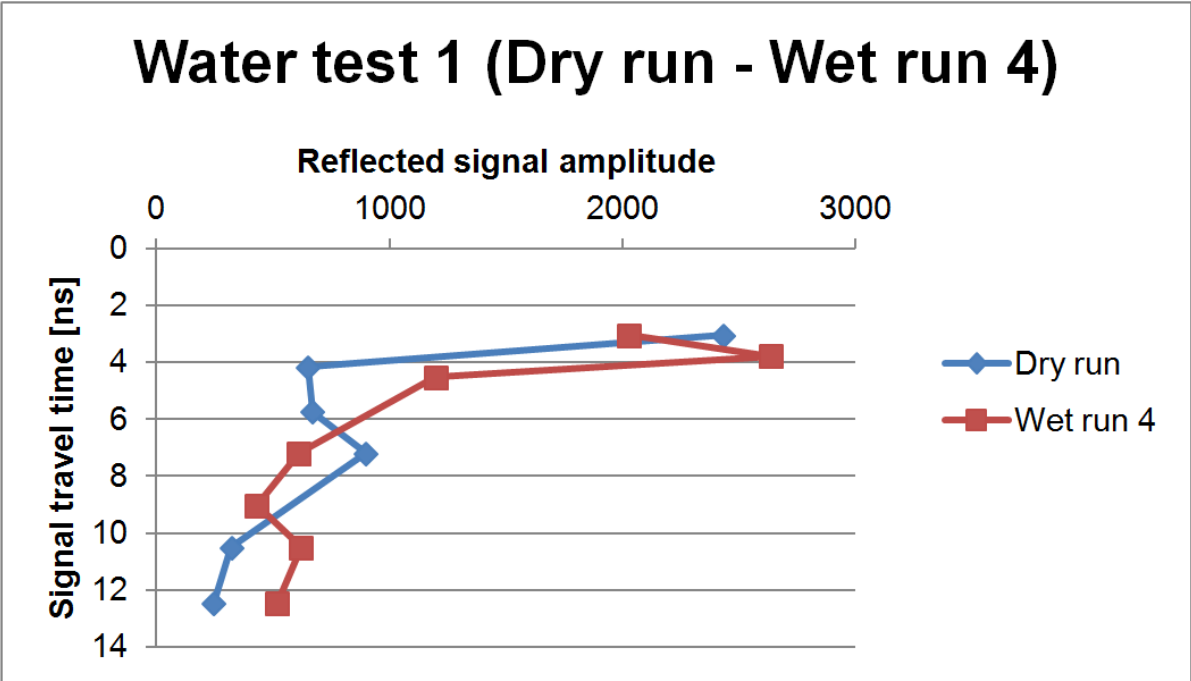

Figure 41: Amplitude time-distribution from dry run to last wet run, 10:35 minutes after water pouring.

Key to understanding the data is to recognise the dry test for its large amplitude peak at the surface, followed by small amplitude peaks further down into the subsurface. While the initial peak amplitude (surface) is lower in the consecutive wet tests, the depth range of large amplitude peaks is increased.

For the time-range of 6-10 nanoseconds, there is a reduction of amplitude values on wet runs compared to those of the initial dry run. This seems to be contrary to the expected results, as no section should become drier as a result of the water pouring. The effect is prevalent across all the wet runs, but could simply be an outlier-value caused by methodological inaccuracies in the dry run.

Of the other plausible causes, most notable is the water pouring method itself. As the water was poured into the ballast, both the amount and velocity of the water far exceeded anything the track had previously been exposed to during normal operation. It is therefore likely that fines and other fouling material was washed out of the ballast, leaving a cleaner, less fouled ballast for the wet runs of the test. As clean ballast has less potential to retain water, it will also have less potential for high dielectric constants and high signal reflection amplitudes. This effect would have less impact deeper into the ballast and subgrade layers. As such, it could also have contributed to the apparent drop in signal reflection amplitude seen at surface level (3.052 ns) from dry run to the first wet runs.

Another interesting feature of the wet run values of site (a) is the apparent pooling of water occurring around 10.5 ns. This is most likely caused by the water being hindered by less permeable mediums, e.g. going from ballast to subgrade. The ballast thickness at the site is estimated to be approximately 0.5 m. Assuming the ballast fouling condition as lightly spent wet ballast, table 1 indicates a wave propagation velocity of approximately 1.40×10^8 m/s. This gives the following travel time of the signal:

$$d = v(\frac{t}{2})$$
$$0.5m = 1.40 \times 10^8 m/s(\frac{t}{2})$$
$$t = \frac{2 \times 0.5m}{1.40 \times 10^8 m/s}$$
$$t = 7.143ns$$

The difference in signal travel time between surface reflections and the indicated pooling of water is $10.498\ ns - 3.052\ ns = 7.446\ ns$. The calculated t-value and the registered time of water pooling are very similar, indicating that the pooling of water is in fact occurring at the transition from ballast to subgrade.

Uncertainties

From the trends seen in the amplitude data there seems to be a clear ability for the GPR system to register both depth and magnitude of changes in water content in a railway track body. However, the data collected from site (a) also contains data that cannot be directly attributed to the assumed behaviour of water in ballast, or the manual reading of the software results.

- The surface amplitude values (at 3.052 ns) seen in table 7 are highly fluctuating between wet runs. As these were not disturbed in the time between wet runs, they should remain more or less similar. This could be caused by methodological inaccuracies, where each scan is not performed over the exact same spot, but may be a few cm off.

- Although the overall trend is mostly as expected, not all amplitude development follows the norm, but fluctuate back and forth between scanning runs. This can be seen from the graphs in appendix B

Control test, site (b)

To assess the scope of normal variations for amplitude values, several control tests were performed. First was the data collected for site (b), which was in the same ballast crib, but opposite side (left) from the water pouring site (a).

Water distribution test 1		Channel: 11		Control test, left side (dry) (b)					
Time after pouring [mm:ss]:		01:40		03:50		06:35		10:35	
Dry		Wet run 1		Wet run 2		Wet run 3		Wet run 4	
Amplitude	Time [ns]	Amplitude	Time [ns]	Amplitude	Time [ns]	Amplitude	Time [ns]	Amplitude	Time [ns]
3604	3.052	3455	3.052	3449	3.052	2440	2.930	2550	2.930
2850	4.272	2548	3.906	2993	4.272	3771	3.174	3973	3.174
1172	5.005	2668	4.272	939	5.005	2002	3.784	1955	3.906
883	5.371	762	5.005	670	5.371	864	4.272	1057	4.272
798	6.958	802	6.958	509	7.690	652	6.226	919	5.127
421	7.690	598	7.690	725	9.399	515	7.324	564	6.226
615	9.399	511	9.644	419	12.573	262	10.254	582	7.202
295	12.573	563	12.573					350	

Table 8: Time and amplitude values for water distribution test 1, site (b)

The values in table 8 were expected to be unchanged between runs, with an exception for values from deep layers, as the water is expected to also distribute outwards as it percolates down through the track body. Yet there are several signal travel times whose amplitudes vary significantly between runs.
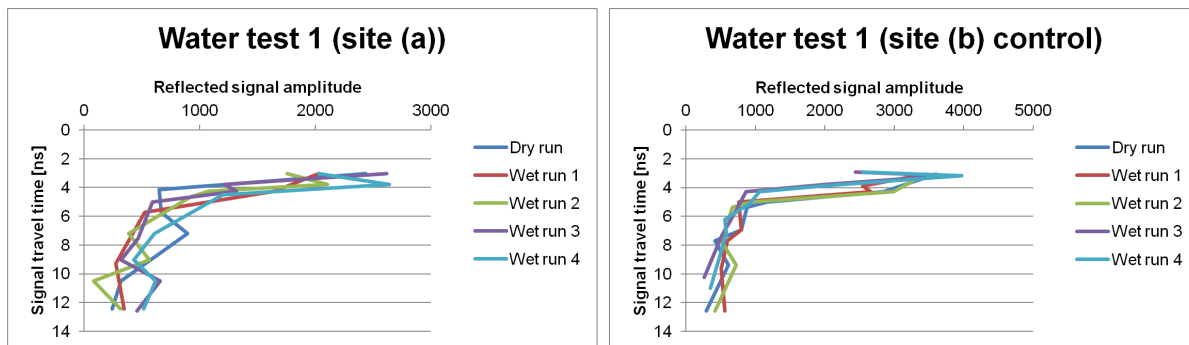
Figure 42: Left: All amplitude data values for site (a) in water dist. test 1. Right: All amplitude data values for site (b) in water dist. test 1.

A graphic manifestation of the amplitude data illustrates that the values still vary between runs, although not nearly as much as in site (a). The variations in amplitude values from site (b) also does not seem to be constrained to the lower depths, where water from site (a) could have contributed to the variations. From this, it is difficult to determine exactly how much of the variation is due to the measuring method, and how much is due to site (b) being affected by water poured at site (a).

Control test, site (c)

A second control was performed at site (c), in the middle of a ballast crib far enough away from the water pouring site to avoid being affected by any activity there.

Water distribution test 1		Channel: 14		Control test outside of wet area (c)					
Time after pouring [mm:ss]:		01:40		03:50		06:35		10:35	
Dry		Wet run 1		Wet run 2		Wet run 3		Wet run 4	
Amplitude	Time [ns]	Amplitude	Time [ns]	Amplitude	Time [ns]	Amplitude	Time [ns]	Amplitude	Time [ns]
4287	3.052	3983	3.052	3810	3.052	3779	3.052	4179	3.052
3209	3.906	2870	3.906	2157	3.906	2837	3.906	2927	3.906
2773	4.272	1963	4.272	1936	4.272	2256	4.272	2467	4.272
1176	5.005	1033	4.761	921	5.005	1261	4.761	1329	5.005
790	6.103	1006	5.005	769	6.103	483	5.859	843	6.103
652	6.592	564	6.103	787	6.470	448	6.592	688	6.470
644	8.057	416	6.592	529	8.301	524	8.179	616	8.057
447	10.254	419	8.301			397	10.254	399	10.254
		398	10.254						

Table 9: Time and amplitude values for water distribution test 1, site (c)

As site (c) was not affected by water, it is obvious from the numbers in table 9 that surface values may vary greatly, even without being affected by anything outside of the measuring method itself. There is also no pattern between sites in the way each run's surface values vary, which could have attributed the variations to factors related to the conduction of each run (e.g. water pumping from track loading by the surveying vehicle).

An important discerning difference between data from site (c) and site (a) and (b) is that for the former, amplitude peaks are almost always located at the same signal travel times. This indicates that the water pouring in site (a) indeed had an effect on the amplitude peak locations. It is possible to extract data from those times to quantify differences in amplitude values between survey runs. Similar comparisons cannot be done for site (a) and (b) because peaks located at different depths/travel times cannot be assumed to have identical EM properties.
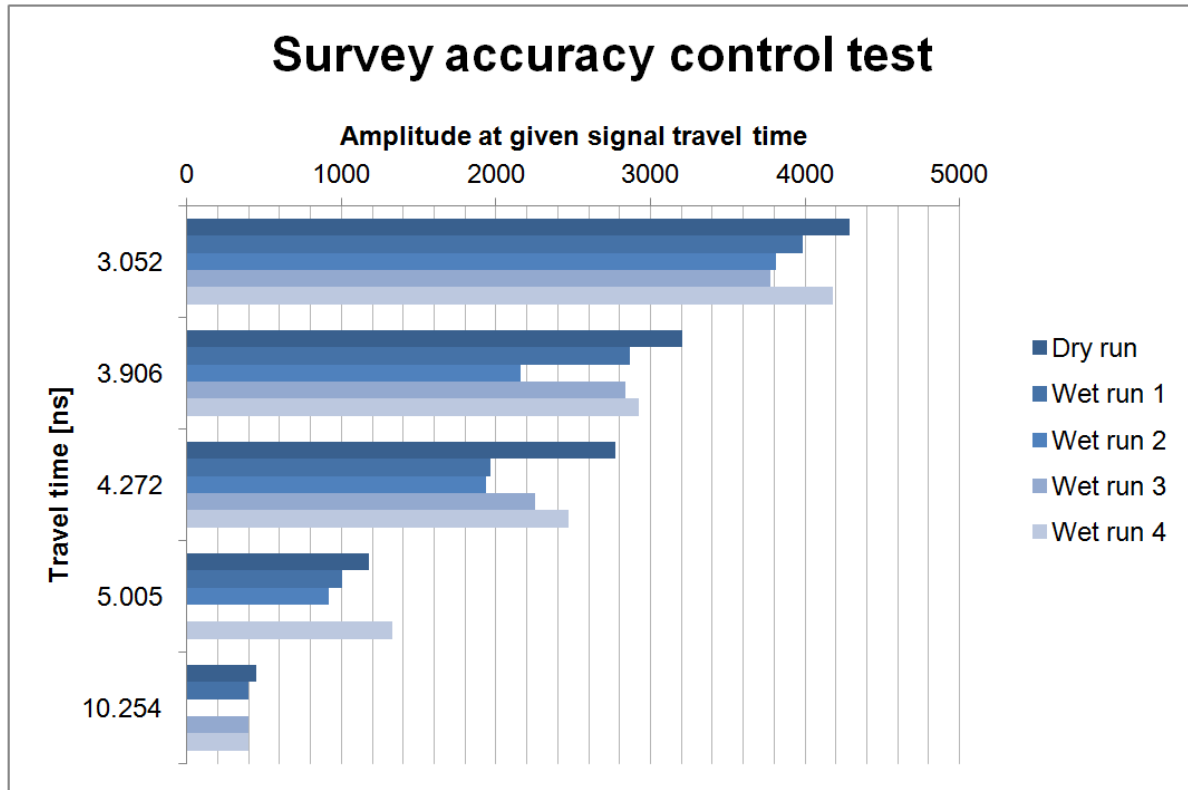
Figure 43: Signal reflection amplitudes at key signal travel times for water dist. test 1, site (c). (Two data points missing due to lack of amplitude peak)

As seen from comparing the amplitude values in fig. 43 there is still a considerable variation in values, even when the actual conditions have not changed. To make sure these variations are not just caused by differences in the initial surface reflection strengths, fig. 44 displays the reflection amplitude values as percentages of initial reflection amplitude. As also this representation shows considerable value variations between scanning runs, it is apparent that the signal either does not attenuate equally between runs or is simply inaccurate in its interpretation of the medium's dielectric contrasts. The variations seem to subside as the signal penetrates deeper into the medium, and values become more similar. It is therefore possible that signals with longer travel times can be viewed as slightly more accurate than those from more shallow reflections.
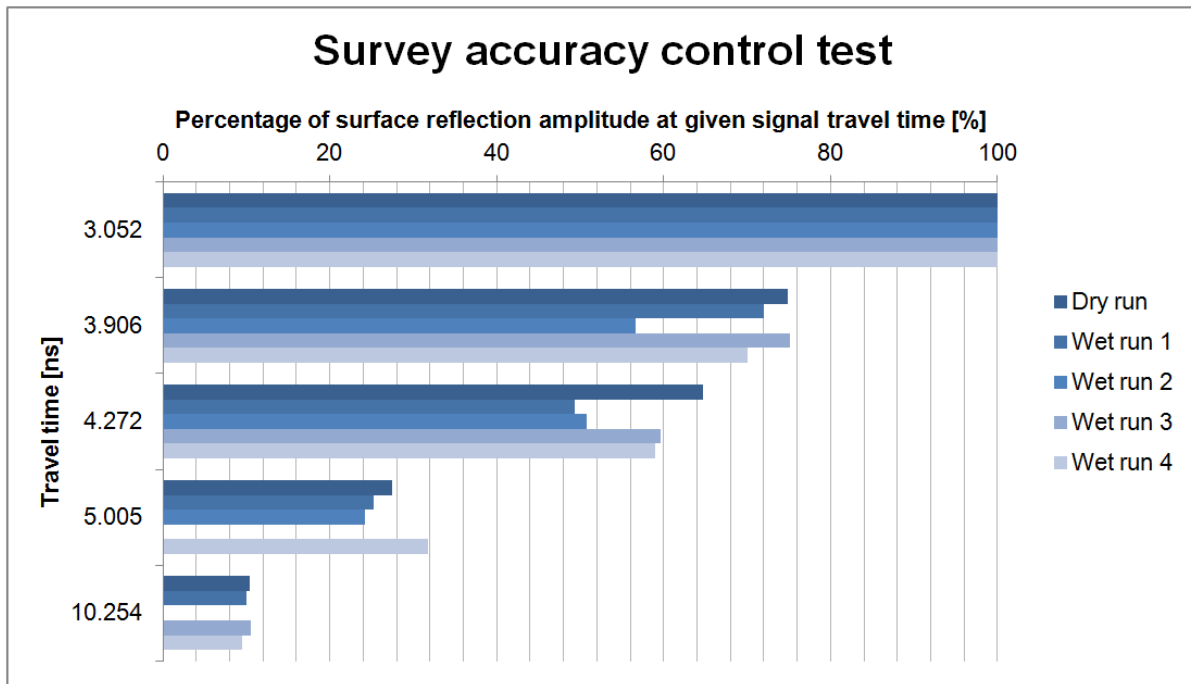
Figure 44: Signal reflection amplitudes at key signal travel times as percentages of initial reflection amplitudes.

The natural variations in the method are therefore substantial, which makes it difficult to draw definite conclusions directly from the data in site (a). However, viewing the data side by side graphically in fig. 45 shows that the water has definitely had an impact on the amplitude values through the subsurface. In addition, the data collected from the control test are a lot more consistent between runs, compared to the data from site (a).
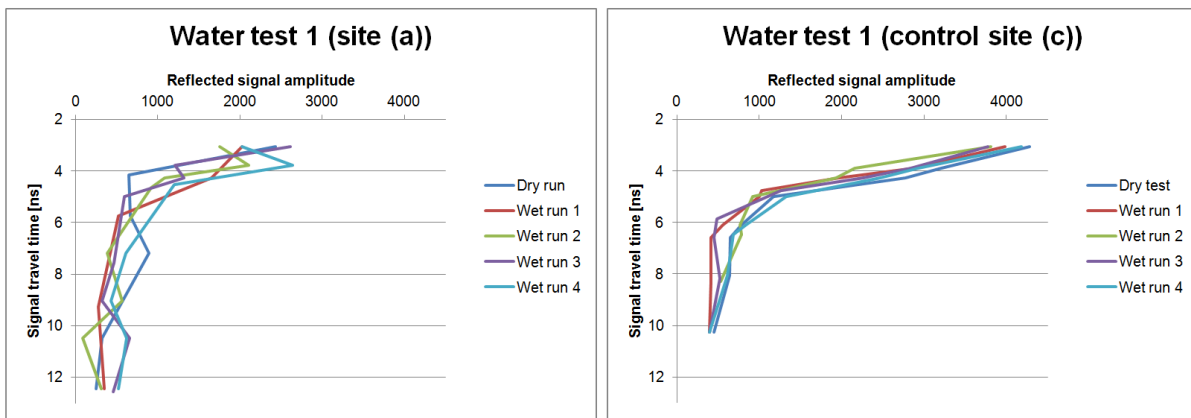

Figure 45: All data points collected for amplitude and time values in water distribution test 1, from site (a) and site (c).

6.2.2 Water distribution test 2

In the second water distribution test, the goal was to register the distribution of water over time and compare it with the results found in the first test. As the mud pumping in the area would have significantly reduced the medium's permeability, the water should percolate at a slower rate than in the cleaner ballast from test 1. As the expected outcome was known, a verification of this through the GPR data would be a great contribution towards proving the GPR's abilities in detecting and mapping water distribution in the track body.

The previously encountered effect where the rapidly poured water could wash out fines from the upper ballast sections is expected to also be a factor in this test, though it is difficult to say with certainty whether the density of the mud will dampen or accentuate this effect.

As a result of time constraints on the line, data was not collected past the time 04:30 after pouring. Comparisons between the two tests must therefore be based on the trends seen within the first 5 minutes after pouring.

Water distribution test 2		Channel: 11					
Time after pouring [mm:ss]:		01:00		02:25		04:30	
Dry		Wet run 1		Wet run 2		Wet run 3	
Amplitude	Time [ns]	Amplitude	Time [ns]	Amplitude	Time [ns]	Amplitude	Time [ns]
1610	2.930	2406	3.052	1889	3.052	1791	3.052
1471	3.784	2002	4.150	1770	4.072	2405	4.272
2489	4.150	910	5.371	868	7.202	966	7.568
635	6.714	809	7.568	33	13.184	369	10.132
497	11.597	497	10.132			267	13.061
336	14.648	353	13.061				

Table 10: Time and amplitude values for water distribution test 2

While the values may be difficult to interpret directly from the numbers themselves, a stepwise graphic projection aides in describing the development of water distribution over time.
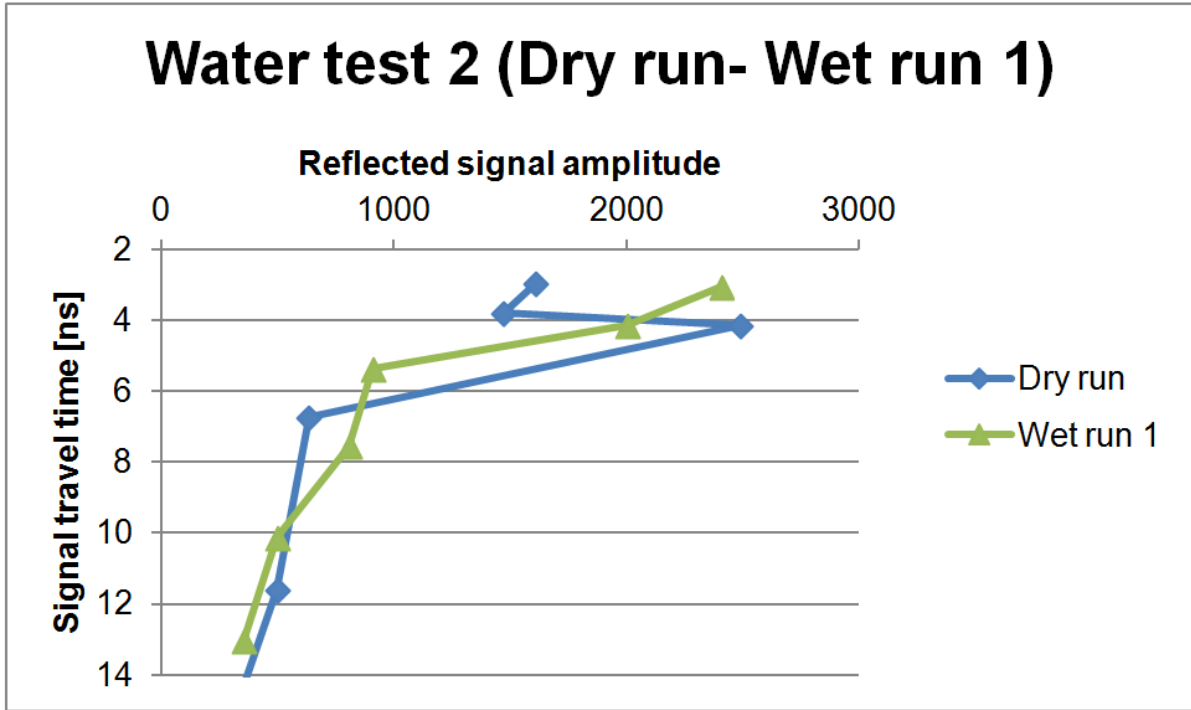
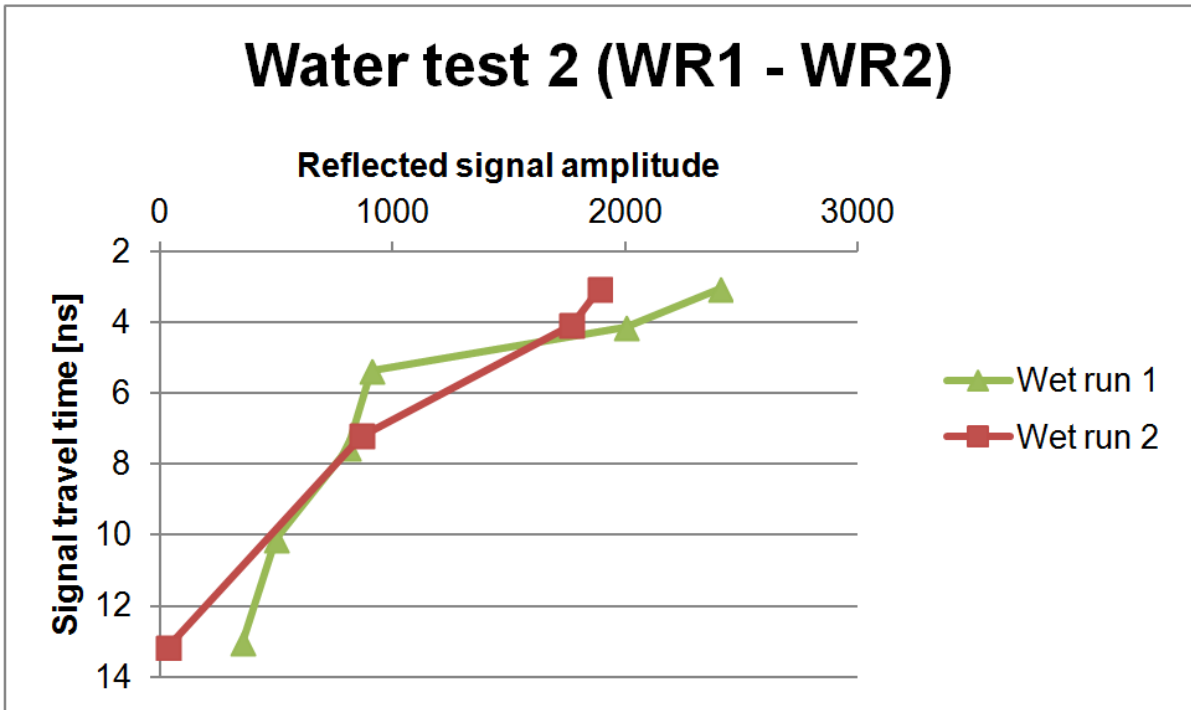Figure 46: Development of amplitude-time data from dry run to first wet run. Water dist. test 2.

Figure 47: Development of amplitude-time data from first wet run to second wet run. Water dist. test 2.
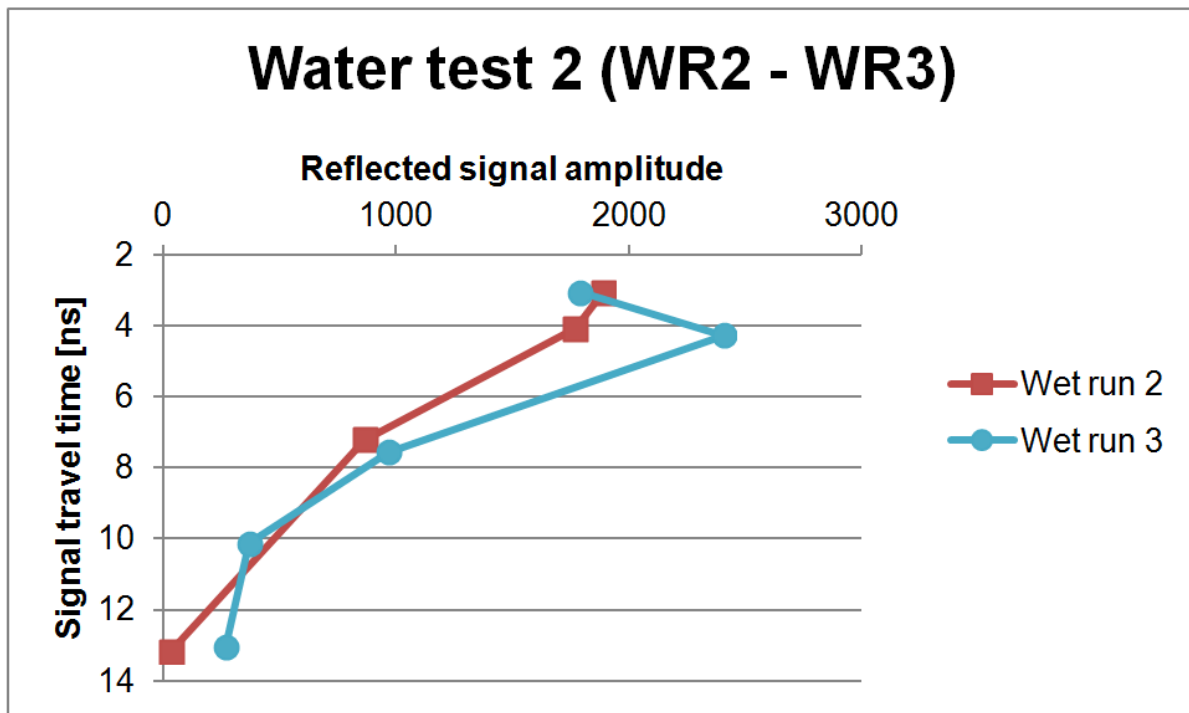
Figure 48: Development of amplitude-time data from second wet run to third wet run. Water dist. test 2

The gradual trend of the water is observable in figs. 46 to 48, where it follows a similar pattern to the ones seen in water distribution test 1. Missing is the apparent pooling of water near the ballast/subgrade interface. This is just as expected since the nature of the fouling will minimise the differences in permeability between the two layers. However, seeing as the scanning in this second test stopped after 04:30, and water pooling was only observed after 06:35 in the first test, this alone is not enough to count as an observable difference between the two tests. As there also is no clear detectable interface of water to accurately detect its propagation down through the ballast, it is not possible to infer anything about the ballast condition from these data alone.

There is also no reason to believe the errors in the second test to be any smaller than those seen in the first test's control. Not all the observed trends in the second scan correspond to predicted or likely movement of water (e.g. the amplitude drop at 13.184 ns in wet run 2), which further indicates the presence of reading errors.
As the muddy slurry which fills the ballast is very good at retaining water, this test most likely suffered due to the wet track conditions on the testing day. The medium would have been nearly saturated with water, to a point where contrasts between "dry" and wet runs were not substantial enough to give unambiguous results.

Wet clayey soils are known to be lossy environments (very high signal attenuation) for EM signals. It would have affected the signal strength of deeper reflections a lot more than what was the case in the first water test. This could explain some of the weak amplitudes registered in the lower parts of the time range, and the subsequent lack of signal development over time.
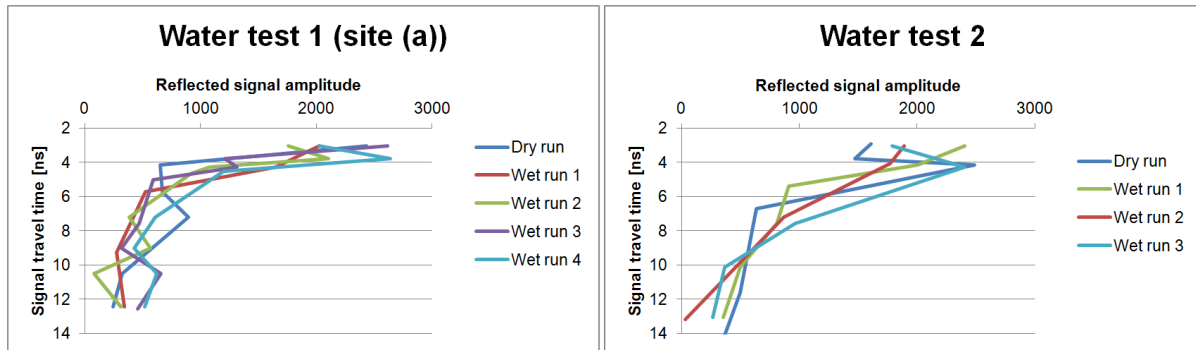

Figure 49: Left: All amplitude data values for site (a) in water dist. test 1. Right: All amplitude data values for water dist. test 2.

A visual comparison of the test results indicates a tendency where reflected signal amplitudes vary slightly more in the upper sections (lower signal travel times) for water test 2, than for water test 1. As these differences seem to appear at lower depths in water test 1, this may be an indication of the expected result, where the cleaner and more permeable ballast lets water through more quickly than the muddy slurry in water test 2.

6.2.3   Remarks

The results gathered from the two water distribution tests suffered under the wet conditions of the track, which caused difficulties discerning the differences between dry and wet runs. Still, overall larger amplitudes are registered for wet runs than for the dry run.

The direct one-to-one comparisons between amplitude values cannot accurately describe the water propagation due to the inherent inaccuracies and value variations in the test. However, the patterns seen from the graphic overview are largely consistent with the expected results from the test, and do represent the trend of water distribution through the ballast body. Especially for the first water test. This has strengthened the hypothesis that water distribution can be mapped from GPR data, but not conclusively confirmed it.

7 Conclusions

From the work in this thesis, it is clear that Ground Penetrating Radar holds much potential for use in railway track inspection. The field surveys proved its ability to collect extensive and accurate data from subsurface features, with minimal data processing and without disturbing the track.

While there were no ballast pockets on the surveyed stretch, the system successfully detected the ballast/subgrade interface, subgrade penetration, mud pumping and deep rock formations. As most track body anomalies will manifest as variations of these, it is very likely that ballast pockets would be detected with this inspection method. Previous studies support this conclusion and have already seen numerous successful detections of ballast/subgrade interface, ballast pockets, subgrade penetration, buried objects and similar feaures. Work is already being done to automatically detect and classify ballast pockets through computer processing of GPR data.

With the accurate detection of ballast/subgrade interface, ballast fouling condition can be approximated from simple signal travel-time comparisons. From the literature review it is also apparent that data interpretation techniques have come a long way the last ten years. Advanced signal processing can now extract more information from the GPR signal, enabling detailed information on moisture content and the distribution and level of fouling. The opportunities for automatic classification and color coding are likely to drastically reduce interpretation times and room for subjective human error.

The GPR's ability to map water distribution was all but confirmed from the theory, with several successful cases of moisture detection based on advanced post-processing of signals. However, field study results from this thesis proved only partly conclusive. There were visible differences between scans of wet ballast compared to dry ballast. Nevertheless, while the overall pattern of results were as expected, the inherent value variations within the test were too large to decisively confirm the ability based on this test alone. This was likely caused by unfavourable track conditions (already wet track).

It is therefore possible to use Ground Penetrating Radar to detect anomalies such as ballast pockets in railway ballast. It is most likely also possible to map the distribution of water in the ballast, as this was supported by the theory, but no definite answer was given from the field study.

7.1 Future work

To further advance and build upon the discoveries of this thesis, several subjects should be explored further.

- Perform the water distribution test on confirmed dry track body (or in laboratory) to better differentiate between dry and wet scans. Also recommended to perform the test without moving the surveying rig between scans, to guarantee longitudinal consistency of the scanning site. (Not possible with the equipment used in this test).

- Test surveys should also be attempted on dry track to assess the impact of water in this test survey.

- Excavate core samples of surveyed stretch to further confirm the accuracy of the scans.

- Perform surveys on closed track sections where full scale ballast pockets can be implemented and surveyed.

- Survey for animal burrow detection on actual known cases of burrows.

- Design automation procedures for time savings in GPR data interpretation.

- Attempt practical application of the ballast void scattering method and the scattering amplitude method. The successful application of this method would be valuable for many railway lines with poor quality gravel sub-ballast in Norway.

- Further explore the extent of detectable track anomalies and faults with GPR.

References

3d-radar (2009). *GeoScope ᵀᴹUser's Manual Model GS3F.*

Al-Qadi, I., Xie, W., Jones, D., and Roberts, R. (2010a). *Development of a time-frequency approach to quantify railroad ballast fouling condition using ultra-wide band ground-penetrating radar data. International Journal of Pavement Engineering*, 11.

Al-Qadi, I., Xie, W., and Roberts, R. (2008). *Scattering analysis of ground-penetrating radar data to quantify railroad ballast contamination. NDT & E International*, 41.

Al-Qadi, I., Xie, W., Roberts, R., and Leng, Z. (2010b). *Data Analysis Techniques for GPR used for Assessing Railroad Ballast in High-Frequency Environment. Journal of Transportation Engineering*, 136.

Annan, A. P. (2003). *Ground Penetrating Radar Principles, Procedures & Applications.* Sensors & Software Inc.

Annan, A. P. (2009). *Ground Penetrating Radar Theory and Applications.* chapter 1. Electromagnetic Principles of Ground Penetrating Radar. Elsevier. Editor: Harry M. Jol.

Ayala-Cabrera, D., Campbell, E., Carreño Alvarado, E. P., and Izquierdo, J. (2014). *Water Leakage Evolution Based on GPR Interpretations. Procedia Engineering*, 89.

Brough, M., Stirling, A., Ghataora, G., and Madelin, K. (2003). *Evaluation of railway trackbed and formation: a case study. NDT & E International*, 36.

Carpenter, D., Jackson, P. J., and Jay, A. (2004). *Enhancement of the GPR method of railway trackbed investigation by the installation of radar detectable geosynthetics. NDT & E International*, 37.

Cassidy, N. J. (2009). *Ground Penetrating Radar Theory and Applications.* chapter 2. Electrical and Magnetic Properties of Rocks, Soils and Fluids. Elsevier. Editor: Harry M. Jol.

Clark, M. (2001). Non-destructive and geotechnical testing of railway track bed ballast. PhD thesis, University of Edinburgh.

Clark, M., Gordon, M., Giannopoulos, A., and Forde, M. (2004). *Advanced analysis of ground penetrating radar signals on railway. In Proceedings of the 7th International Conference on Railway Engineering, London, UK.*

Clark, M. R., Gillespie, R., Kemp, T., McCann, D. M., and Forde, M. C. (2001). *Electromagnetic properties of railway ballast. NDT & E International*, 34.

Daniels, D. J. (2004). *Ground Penetrating Radar, 2nd Edition*. The Institution of Electrical Engineers.

De Bold, R., O'Connor, G., Morrissey, J. P., and Forde, M. C. (2015). *Benchmarking large scale GPR experiments on railway ballast. Construction and Building Materials*, 92.

Eide, E., Hoff, I., and Værnes, E. (2001). *Undersøkelse av ballast under jernbane ved hjelp av georadar*. Technical report, SINTEF.

El Said, M. A. H. (1956). *Geophysical prospection of underground water in the desert by means of electromagnetic interference fringes*.

Fontul, S., Fortunato, E., and De Chiara, F. (2014). *Evaluation of ballast fouling using GPR*. Technical report. 15th International Conference on Ground Penetrating Radar.

Gallagher, G. P., Leiper, Q., Williamson, R., Clark, M. R., and Forde, M. C. (1999). *The application of time domain ground penetrating radar to evaluate railway track ballast. NDT & E International*, 32.

Göbel, C., Hellmann, R., and Petzold, H. (1994). *Georadar-model and in-situ investigations for inspection of railway tracks*. Technical report, Fifth International Conferention on Ground Penetrating Radar.

Grote, K., Hubbard, S., Harvey, J., and Rubin, Y. (2005). *Evaluation of infiltration in layered pavements using surface GPR reflection techniques. Journal of Applied Geophysics*, 57.

Hay, W. (1982). *Railroad Engineering*. Wiely-Interscience.

Hugenschmidt, J. (2000). *Railway track inspection using GPR. Journal of Applied Geophysics*, 43.

Hyslip, J. P., Olhoeft, G. R., Smith, S. S., and Selig, E. T. (2005). *Ground Penetrating Radar for Railroad Track Substructure Evaluation*. Technical report. U.S. Department of Transportation.

Indraratna, B., Salim, W., and Rujikiatkamjorn, C. (2011). *Advanced Rail Geotechnology - Ballasted Track*. CRC Press/Balkema.

Jack, R. and Jackson, P. (1999). *Imaging attributes of railway track formation and ballast using ground probing radar. NDT & E International*, 32.

Jernbaneverket. *Map of railway infrastructure.* `http://customapps2.geodataonline.no/Jernbaneverket/kartinnsyn/` [Accessed 2015].

Keogh, T., Mesher, D. E., and Keegan, T. R. (2006). *An Integrated System for Accurate Tie and Ballast Condition Assessment.* AREMA Conference.

Kind, T. (2011). *GPR Antenna Array for the Inspection of Railway Ballast. Proceedings of the National Seminar & Exhibition on Non-Destructive Evaluation.*

Lalagüe, A. (2015). Use of Ground Penetrating Radar for Transportation Infrastructure Maintenance. PhD thesis, Norwegian University of Science and Technology.

Leng, Z. and Al-Qadi, I. L. (2010). *Railroad Ballast Evaluation Using Ground-Penetrating Radar. Journal of the Transportation Research Board*, 2159.

Li, D., Hyslip, J., Sussmann, T., and Chrismer, S. (2015). *Railway Geotechnics.* CRC Press.

Li, D., Read, D., Thompson, H., Sussmann, T., and McDaniel, R. (2010). *Evaluation of Ground Penetrating Radar Technologies for Assessing Track Substructure Conditions.* Technical report.

Manacorda, G., Morandi, D., Sarri, A., and Staccone, G. (2001). *A customized GPR system for railroad tracks verification.* Technical report.

Narayanan, R. M., Kumke, C. J., and Li, D. (1999). *Railroad Track Monitoring Using Ground Penetrating Radar: Simulation Study and Field Measurements.* SPIE Conference on Subsurface Sensors and Applications, Denver, Colorado.

Network Rail (2010). *Network Rail Asset Management Policy.* Technical report.

Norge i Bilder. *Satellite photo of survey area.* `http://customapps2.geodataonline.no/Jernbaneverket/kartinnsyn/` [Accessed 2015].

Olhoeft, G. R. and Selig, E. T. (2002). *Ground Penetrating Radar Evaluation of Railway Track Substructure Conditions. Proceedings of SPIE*, 4758.

Oppenheim, A. V., Schafer, R. W., and Buck, J. R. (2005). *Discrete-time Signal Processing.* Pearson Prentice Hall.

Plati, C., Loizos, A., and Papavasiliou, V. (2010). *Inspection of railroad ballast using geophysical method. International Journal of Pavement Engineering*, 11.

RailCorp Network (2009). *TMC 421 - Track Drainage.* Technical report.

Roberts, R., Al-Qadi, I., Tutumluer, E., and Boyle, J. (2009). *Subsurface Evaluation of Railway Track Using Ground Penetrating Radar.* Technical report. U.S. Department of Transportation.

Roberts, R., Rudy, J., Al-Qadi, I., Tutumluer, E., and Boyle, J. (2006). *Railroad Ballast Fouling Detection using Ground Penetrating Radar - A New Approach Based on Scattering from Voids.* Technical report.

Roberts, R., Schutz, A., Al-Qadi, I., and Tutumluer, E. (2007). *Characterizing Railroad Ballast Using GPR: Recent Experiences in the United States.* Technical report.

Selig, E. and Waters, J. (1984). *Track Geotechnology and Substructure Management.* Thomas Telford Publications.

Selig, E. T. and Cantrell, D. D. (2001). *Track Substructure Maintenance–From Theory to Practice.* Technical report, AREMA Annual conference 2001.

Shangguan, P. and Al-Qadi, I. (2014). *Content-based image retrieval approaches to interpret ground penetrating radar data. Construction and Building Materials*, 69.

Shangguan, P., Al-Qadi, I., and Leng, Z. (2012). *Development of Wavelet Technique to Interpret Ground-Penetrating Radar Data for Quantifying Railroad Ballast Conditions. Transportation Research Journal*, 2289.

Shao, W., Bouzerdoum, A., Phung, S. L., Su, L., Indraratna, B., and Rujikiatkamjorn, C. (2011). *Automatic Classification of Ground-Penetrating-Radar Signals for Railway-Ballast Assessment. IEEE Transactions on Geoscience and Remote Sensing*, 49.

Silvast, M., Nurmikolu, A., Wiljanen, B., and Lavomäki, M. (2010a). *An inspection of railway ballast quality using ground penetrating radar in Finland. Journal of Rail and Rapid Transit*, 224.

Silvast, M., Nurmikolu, A., Wiljanen, B., and Lavomäki, M. (2010b). *Identifying frost-susceptible areas on Finnish railways using the ground penetrating radar technique. Journal of Rail and Rapid Transit*, 224.

Su, L., Indraratna, B., and Rujikiatkamjorn, C. (2011). *Non-destructive assessment of rail track condition using ground penetrating radar.* Technical report, IACMAG 2011.

Su, L.-J., Rujikiatkamjorn, C., and Indraratna, B. (2010). *An Evaluation of Fouled Ballast in a Laboratory Model Track Using Ground Penetrating Radar. Geotechnical Testing Journal,* 33.

Sussmann, T. R. (1999). Application of ground penetrating radar to railway track substructure maintenance management. PhD thesis, University of Massachusetts Amherst.

Tzanakakis, K. (2013). *The Railway Track and Its Long Term Behaviour.* Springer.

Uduwawala, D., Norgren, M., Fuks, P., and Gunawardena, A. (2005). *A Complete FDTD Simulation of a Real GPR Antenna System Operating Above Lossy and Dispersive Grounds. Progress In Electromagnetics Research.*
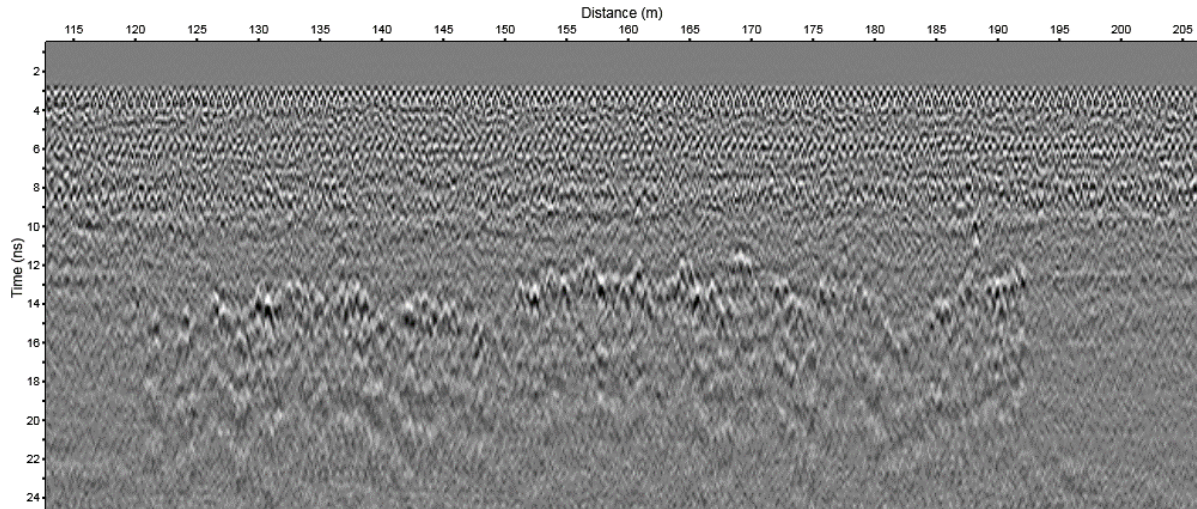
Appendices

A   Scan resolution comparison

Figure 50: Test survey 1 - Sample rate: 1 scan/15 cm
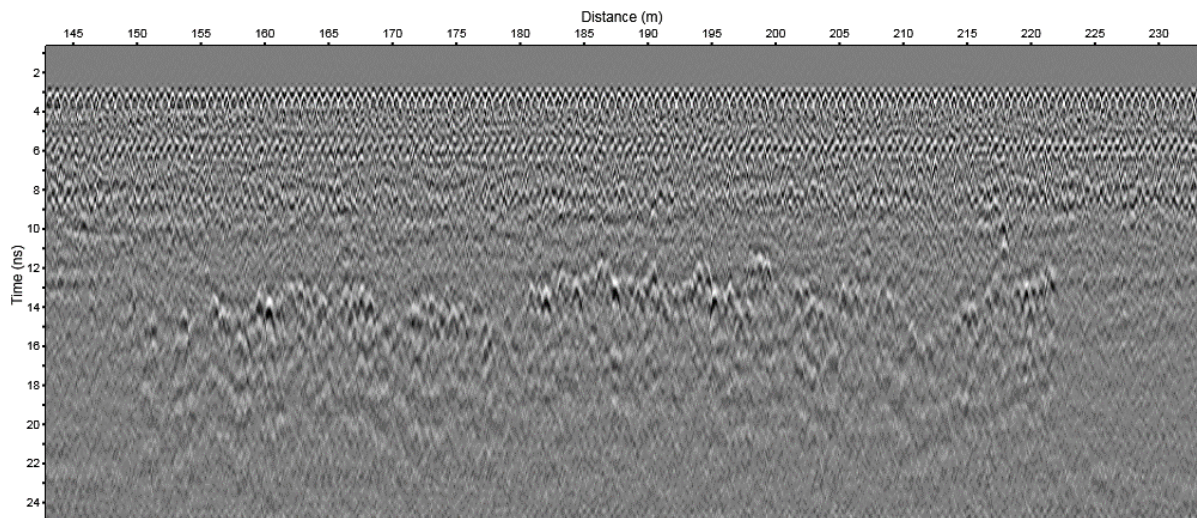

Figure 51: Test survey 2 - Sample rate: 1 scan/10 cm

B   Water distribution test 1.
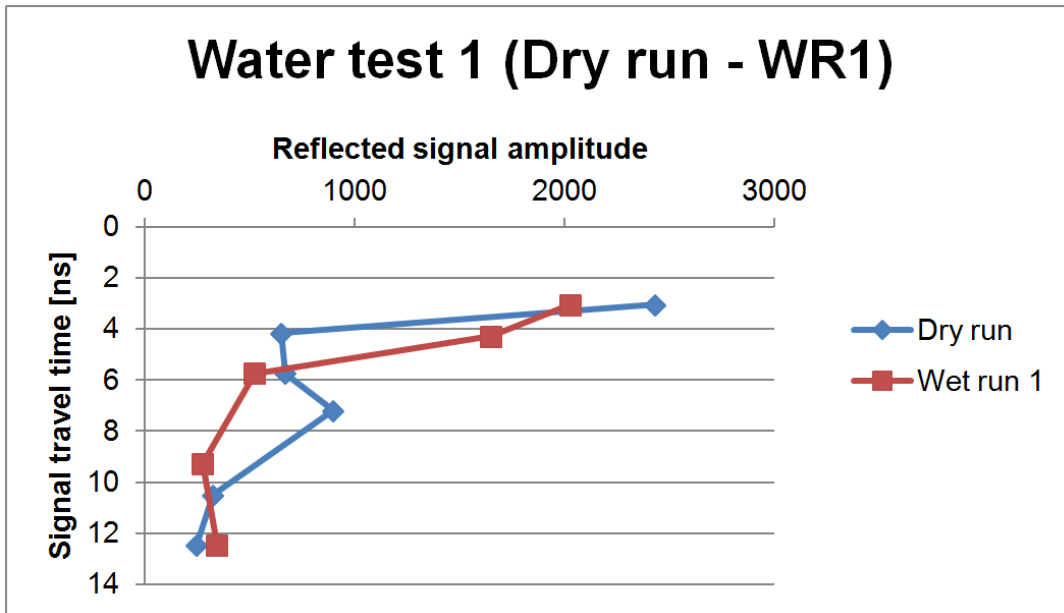## Stepwise amplitude development

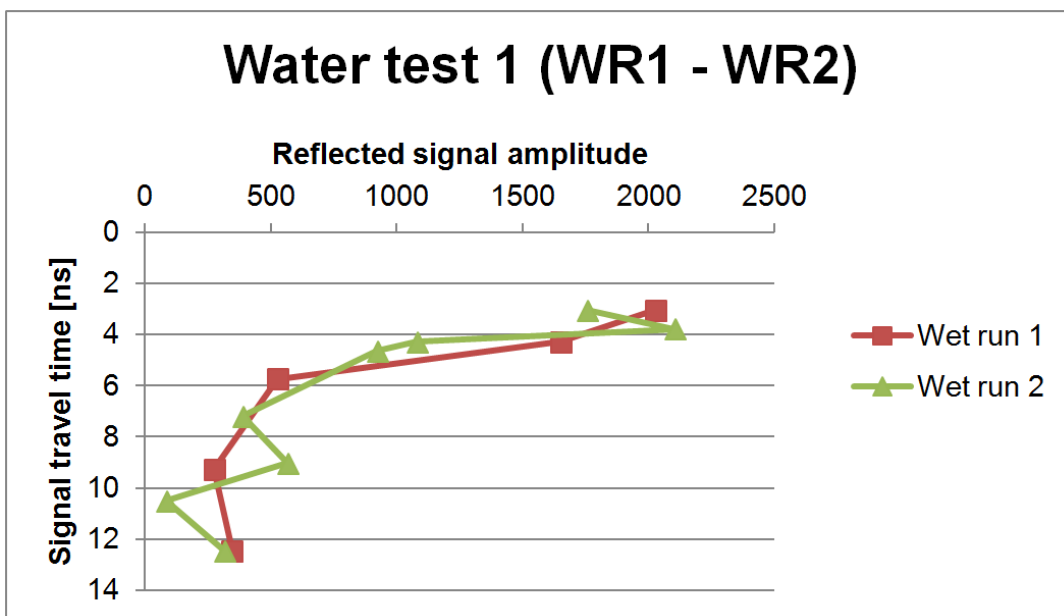Figure 52: Development of amplitude-time data from dry run to first wet run. Site (a)

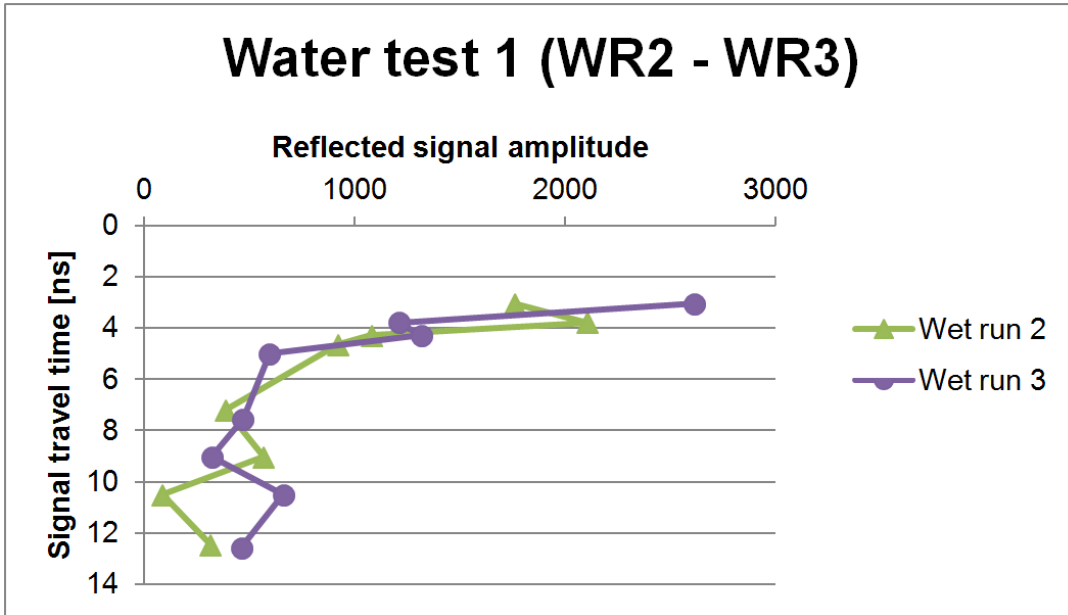Figure 53: Development of amplitude-time data from first wet run to second wet run. Site (a)

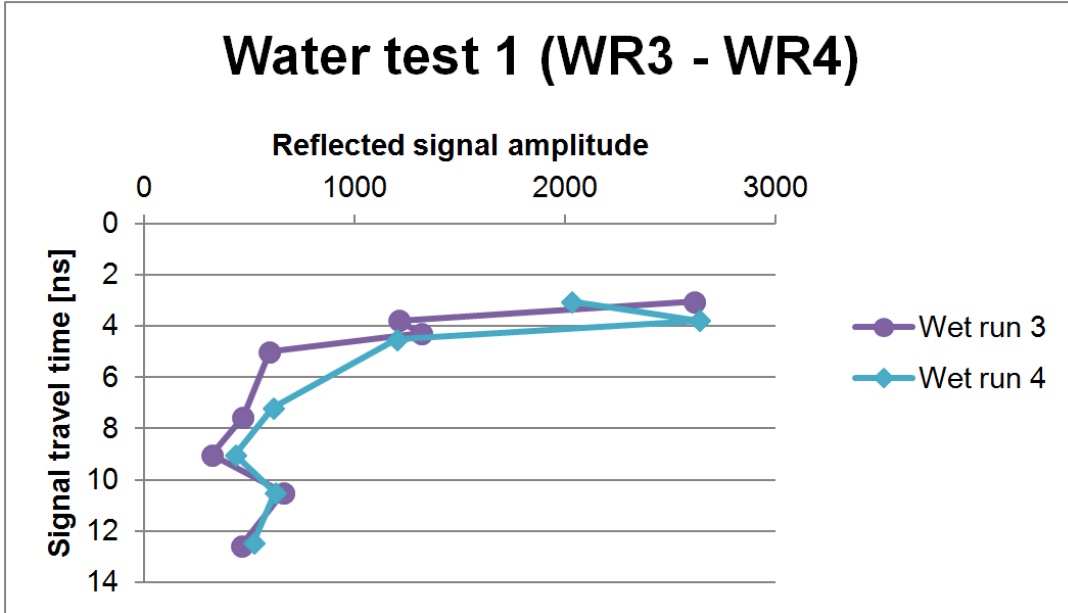Figure 54: Development of amplitude-time data from second wet run to third wet run. Site (a)

Figure 55: Development of amplitude-time data from third wet run to fourth wet run. Site (a)